Supplementary Information

Figure S34. ^{1}H NMR spectroscopic titration experiments of Ni^{2+}. Ni^{2+} was added at at 0, 0.2, 0.4, 0.6, 1.0, 1.2, 1.4 and 2.0 equiv. shown from top to bottom ([Fc-conjugate **5**] = 1mM, CD_3CN)

Figure S35. ^{1}H NMR spectroscopic titration experiments of Cd^{2+}. Cd^{2+} was added at at 0, 0.2, 0.4, 0.6, 1.0, 1.2, 1.4 and 2.0 equiv. shown from top to bottom ([Fc-conjugate **5**] = 1mM, CD_3CN)

Figure S36. ^{1}H NMR spectroscopic titration experiments of Mn^{2+}. Mn^{2+} was added at 0, 0.2, 0.4, 0.6, 1.0, 1.2, 1.4 and 2.0 equiv. shown from top to bottom ([Fc-conjugate **5**] = 1mM, CD_3CN)

Figure S37. ^{1}H NMR spectroscopic titration experiments of Mg^{2+}. Mg^{2+} was added at at 0, 0.2, 0.4, 0.6, 1.0, 1.2, 1.4 and 2.0 equiv. shown from top to bottom ([Fc-conjugate **5**] = 1mM, CD_3CN)

Figure S38. (a) The experimental ESI-MS+ (positive mode) results showing **3** in acetonitrile with the presence of Cd^{2+}. (b) Partial spectrum of the molecular ion of **3**·Cd with an overall of 2+ charge. (c) Theoretical isotopic pattern of the Cd^{2+} complexed to conjugate **3** assigned to [**3** + Cd]$^{2+}$.

Figure S39. (a) The experimental ESI-MS+ (positive mode) results showing **3** in acetonitrile with the presence of Mg^{2+}. (b) Partial spectrum of the molecular ion of **3**·Mg with an overall of 2+ charge. (c) Theoretical isotopic pattern of the Mg^{2+} complexed to conjugate **3** assigned to [**3** + Mg]$^{2+}$.

Figure S40. (a) The experimental ESI-MS+ (positive mode) results showing **3** in acetonitrile with the presence of Mn^{2+}. (b) Partial spectrum of the molecular ion of **3**·Mn with an overall of 2+ charge. (c) Theoretical isotopic pattern of the Mn^{2+} complexed to conjugate **3** assigned to [**3** + Mn]$^{2+}$.

Figure S41. (a) The experimental ESI-MS+ (positive mode) results showing **3** in acetonitrile with the presence of Ni^{2+}. (b) Partial spectrum of the molecular ion of **3**·Ni with an overall of 2+ charge. (c) Theoretical isotopic pattern of the Ni^{2+} complexed to conjugate **3** assigned to [**3** + Ni]$^{2+}$.

Figure S42. (a) The experimental ESI-MS+ (positive mode) results showing **3** in acetonitrile with the presence of Zn^{2+}. (b) Partial spectrum of the molecular ion of **3**·Zn with an overall of 2+ charge. (c) Theoretical isotopic pattern of the Zn^{2+} complexed to conjugate **3** assigned to [**3** + Zn]$^{2+}$.

Figure S43. (a) The experimental ESI-MS+ (positive mode) results showing **4** in acetonitrile with the presence of Cd^{2+}. (b) Partial spectrum of the molecular ion of **4**·Cd with an overall of 2+ charge. (c) Theoretical isotopic pattern of the Cd^{2+} complexed to conjugate **4** assigned to [**4** + Cd]$^{2+}$.

Figure S44. (a) The experimental ESI-MS+ (positive mode) results showing **4** in acetonitrile with the presence of Cu^{2+}. (b) Partial spectrum of the molecular ion of **4**·Cu with an overall of 2+ charge. (c) Theoretical isotopic pattern of the Cu^{2+} complexed to conjugate **4** assigned to [**4** + Cu]$^{2+}$.

Figure S45. (a) The experimental ESI-MS+ (positive mode) results showing **4** in acetonitrile with the presence of Mg^{2+}. (b) Partial spectrum of the molecular ion of **4**·Mg with an overall of 2+ charge. (c) Theoretical isotopic pattern of the Mg^{2+} complexed to conjugate **4** assigned to [**4** + Mg]$^{2+}$.

Figure S46. (a) The experimental ESI-MS+ (positive mode) results showing **4** in acetonitrile with the presence of Mn^{2+}. (b) Partial spectrum of the molecular ion of **4**·Mn with an overall of 2+ charge. (c) Theoretical isotopic pattern of the Mn^{2+} complexed to conjugate **4** assigned to [**4** + Mn]$^{2+}$.

Figure S47. (a) The experimental ESI-MS+ (positive mode) results showing **4** in acetonitrile with the presence of Ni^{2+}. (b) Partial spectrum of the molecular ion of **4**·Ni with an overall of 2+ charge. (c) Theoretical isotopic pattern of the Ni^{2+} complexed to conjugate **4** assigned to [**4** + Ni]$^{2+}$

Figure S48. (a) The experimental ESI-MS+ (positive mode) results showing **5** in acetonitrile with the presence of Cd^{2+}. (b) Partial spectrum of the molecular ion of **5**·Cd with an overall of 2+

charge. (c) Theoretical isotopic pattern of the Cd^{2+} complexed to conjugate **5** assigned to [**5** + Cd]$^{2+}$.

Figure S49. (a) The experimental ESI-MS+ (positive mode) results showing **5** in acetonitrile with the presence of Mg^{2+}. (b) Partial spectrum of the molecular ion of **5**·Mg with an overall of 2+ charge. (c) Theoretical isotopic pattern of the Mg^{2+} complexed to conjugate **5** assigned to [**5** + Mg]$^{2+}$.

Figure S50. (a) The experimental ESI-MS+ (positive mode) results showing **5** in acetonitrile with the presence of Mn^{2+}. (b) Partial spectrum of the molecular ion of **5**·Mn with an overall of 2+ charge. (c) Theoretical isotopic pattern of the Mn^{2+} complexed to conjugate **5** assigned to [**5** + Mn]$^{2+}$.

Figure S51. (a) The experimental ESI-MS+ (positive mode) results showing **5** in acetonitrile with the presence of Ni^{2+}. (b) Partial spectrum of the molecular ion of **5**·Ni with an overall of 2+ charge. (c) Theoretical isotopic pattern of the Ni^{2+} complexed to conjugate **5** assigned to [**5** + Ni]$^{2+}$.

Figure S52. (a) The experimental ESI-MS+ (positive mode) results showing **5** in acetonitrile with the presence of Zn^{2+}. (b) Partial spectrum of the molecular ion of **5**·Zn with an overall of 2+ charge. (c) Theoretical isotopic pattern of the Zn^{2+} complexed to conjugate **5** assigned to [**5** + Zn]$^{2+}$.

Figure S53. UV spectra of Fc-conjugate **3**, **4**, and **5**

Figure S54. Two-dimensional ^{1}H-^{1}H NOEY NMR spectrum of Fc[CO-His(Trt)-His(Trt)-OMe]$_2$ (**3**)

Table S1. Summary of specific angles (°) for the X-ray crystal structures

Table S2. Summary of crystallographic data for Fc-conjugates **4** and **5**.

Table S3. Torsion Angles (deg) for **4** and **5**

Table S4. CV results of 1 mM compound **3**, **4** and **5** under different scan rates in CH$_3$CN (0.1 M TBAP as electrolyte)

Table S5. Electrochemical properties of Fc-peptides **3-5**.

Table S6. Summary of electrochemical data

Table S7: Results of the high resolution electrospray mass spectrometry analysis of acetonitrile solutions containing Fc-conjugates **3** and **5** the absence and presence of metal ions.

Table S8. Summary of IR stretching frequencies (cm^{-1})

Table S9: UV and CD spectroscopic parameters for Fc–peptide conjugate **3** and **5**

Figure S1. The molecular structure of Fc[CO-His(Trt)-Asp(OMe)-OMe]$_2$, **4** with displacement ellipsoids drawn at 30% probability level. Hydrogen-bonding interactions of crystallographically independent molecules A (a) and B (b) as acquired from single-crystal X-ray diffraction studies of Fc-conjugate **4** (d[N(1A)···O(8A)] = 3.000 Å and (d[N(5A)···O(2A)] = 2.954 Å for molecule A, while d[N(5B)···O(2B)] = 3.042 Å and d[N(1B)···O(8B)] = 3.282 Å for molecule B). Dihedral angle (ω) between the two ring-bound substituents of Fc core is shown in (c) with the value of ω is 73.3 for molecule A and (d) 76.0° for molecule B, which both suggests *P*-1,2′ "Herrick conformation". (e) Intermolecular hydrogen bonding interactions at supramolecular level between symmetry related molecule A is d[N(2A)··· N(7A*1)] = 2.967 Å and d[N(6A)···N(3A*2)] = 2.976 Å while, d[N(2B)··· N(7B*3)] = 3.000 Å and d[N(6B)···N(3B*4)] = 2.931 Å for molecule B. For clarity, trityl groups were removed from His residue as well, only intra- and intermolecular hydrogen bonds involving the asymmetric unit are displayed. H atoms bonded to C atoms are not presented, and the H-bond acceptor O atoms are labelled.

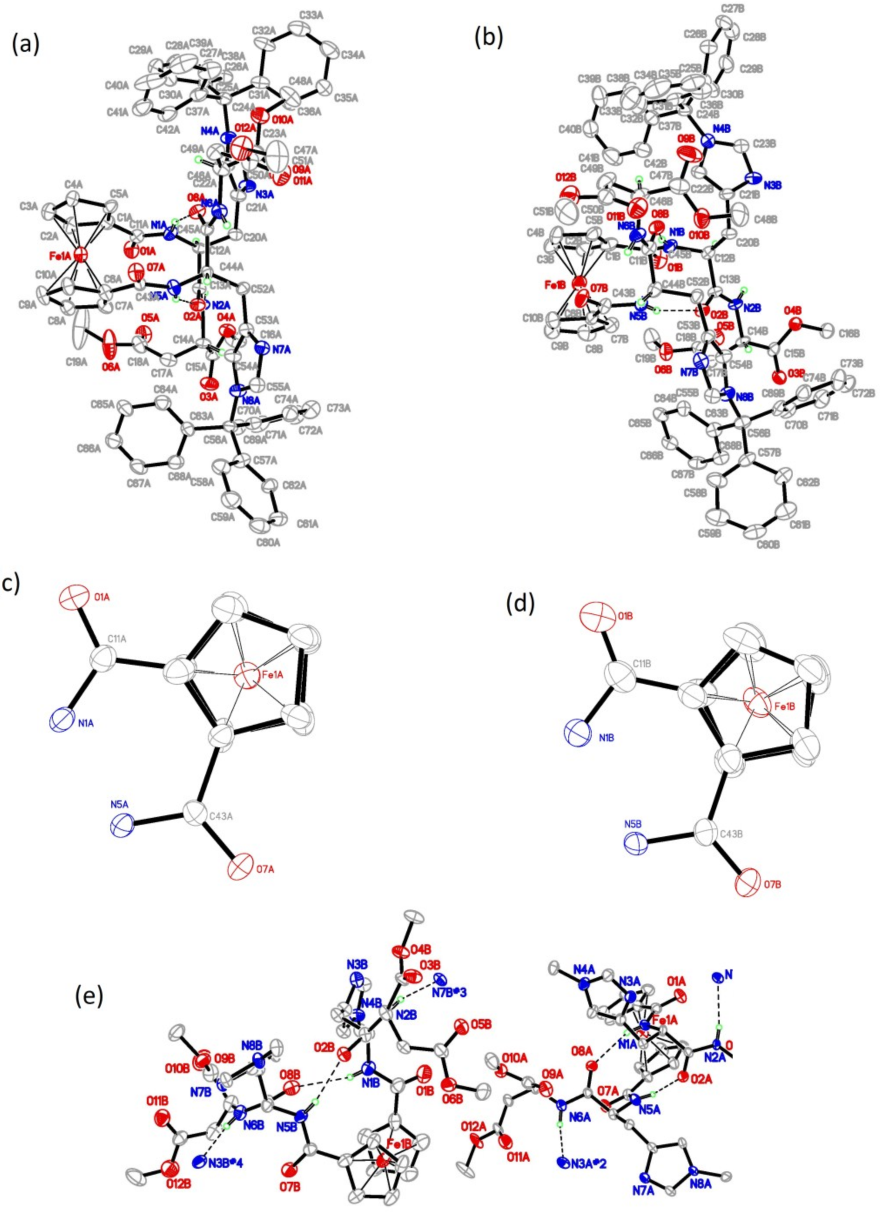

Figure S2. Diagram depicting the crystal structure of Fc[CO-His(Trt)-Glu(OMe)-OMe]$_2$, **5** showing hydrogen bonds as dashed lines. Displacement ellipsoids drawn at 30% probability level. Hydrogen-bonding interactions of crystallographically independent molecules A (a) and B (b) as acquired from single-crystal X-ray diffraction studies of Fc-conjugate **5** (d[N(5A)···O(2A)] = 2.975 Å and d[N(1A)···O(8A)] = 2.978 Å for molecule A, whereas d[N(5B)···O(2B)] = 3.191 Å and d[N(1B)···O(8B)] = 3.019 Å for molecule B). (c) Fc core conformation suggests *P*-1,2′ "Herrick conformation" due to the value of ω is 76.8 and (d) 74.8° for molecule B (e) Intermolecular hydrogen bonding interactions (d[N(6A)··· N(3B)] = 2.956 Å and d[N(7A)···N(2B)] = 2.872 Å) at supramolecular level. For clarity, trityl groups were removed from His residue as well, only intra- and intermolecular hydrogen bonds involving the asymmetric unit are displayed. H atoms bonded to C atoms are not presented, and the hydrogen bond acceptor O atoms are labelled.

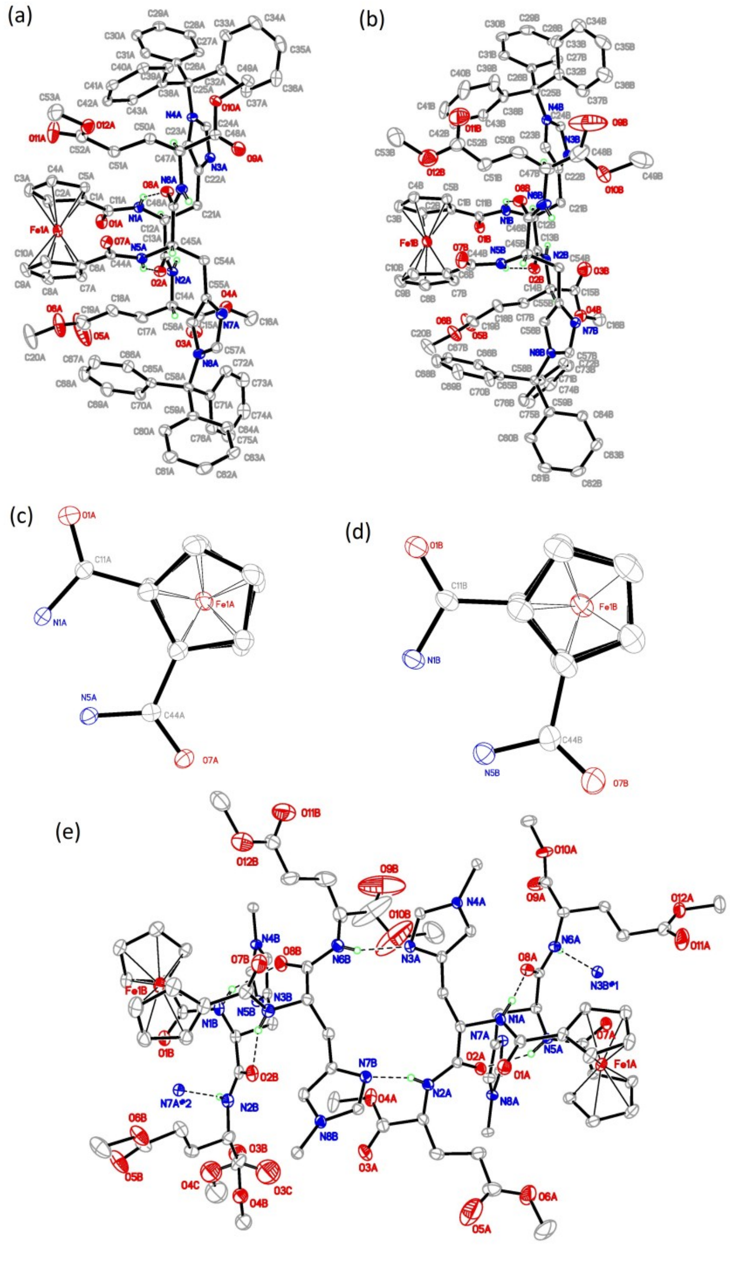

Figure S3. The molecular structures of Fc[CO-His(Trt)-Glu(OMe)-OMe]$_2$, **5** depicting independent molecule A (a) and (b) B. Intramolecular hydrogen-bonding interactions of crystallographically independent molecules as acquired from single-crystal X-ray diffraction studies of Fc-conjugate **5** (d[N(1A)···O(8A)] = 2.978 Å for molecule A, while d[N(5B)···O(2B)] = 3.191 Å and d[N(1B)···O(8B)] = 3.019 Å for molecule B). Trityl groups were removed for clarity from His residues. Only intramolecular hydrogen bonds involving the asymmetric unit are displayed. H atoms bonded to C atoms are not shown, and the H-bond acceptor O atoms are labelled.

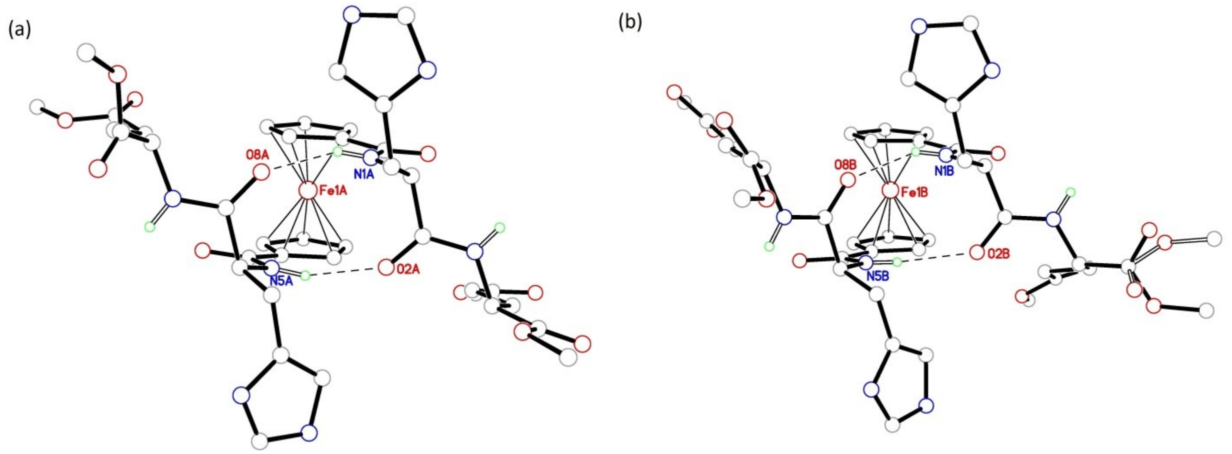

Figure S4. Helically ordered molecular arrangement was formed in the crystal packing of the side viewpoint **4** (a). Depicts Fc-conjugate **4** (of only molecule B) packed in a novel helically ordered arrangement with one turn of 30.33 Å pitch height, within which the distance between the closest ferrocene units is 13.95 Å. Crystal packing of Fc-peptide conjugate **4** showcasing the helical arrangement of upper viewpoint (b). Two intramolecular hydrogen bonds induce an ordered structure together with intermolecular hydrogen bonding.

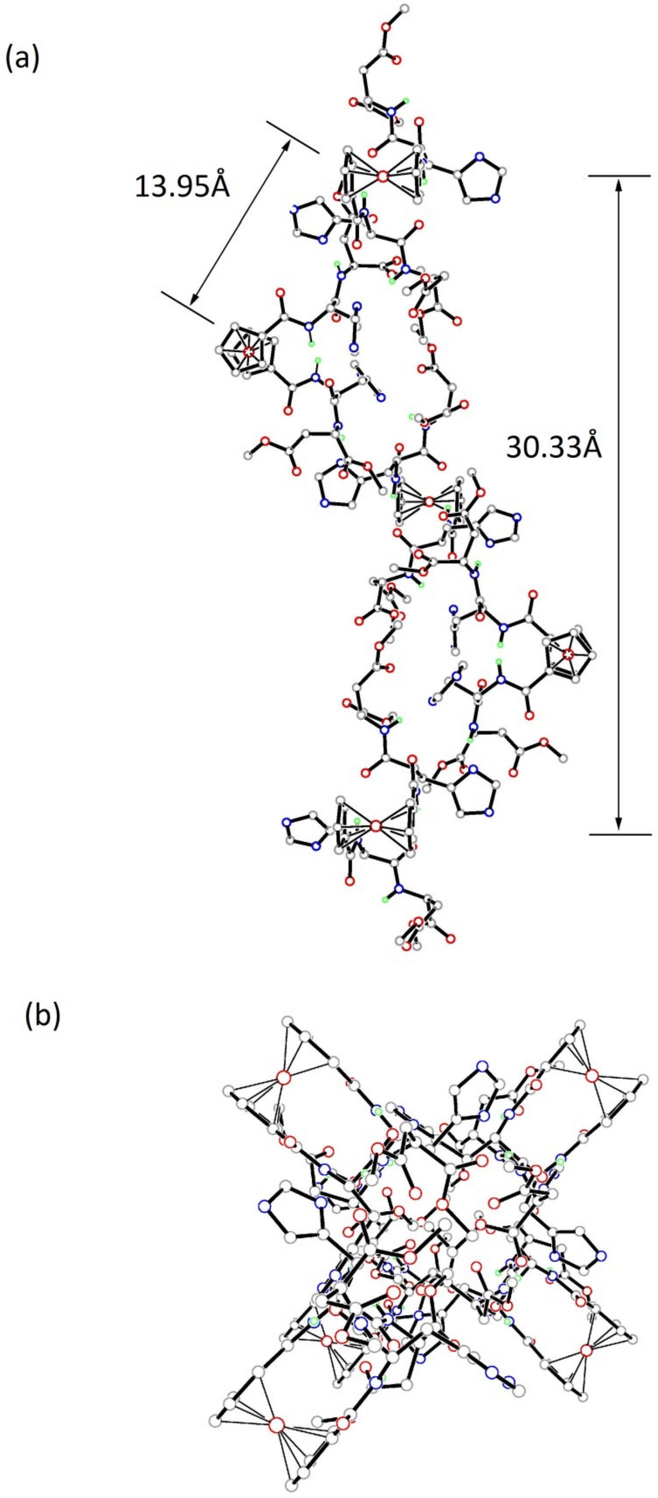

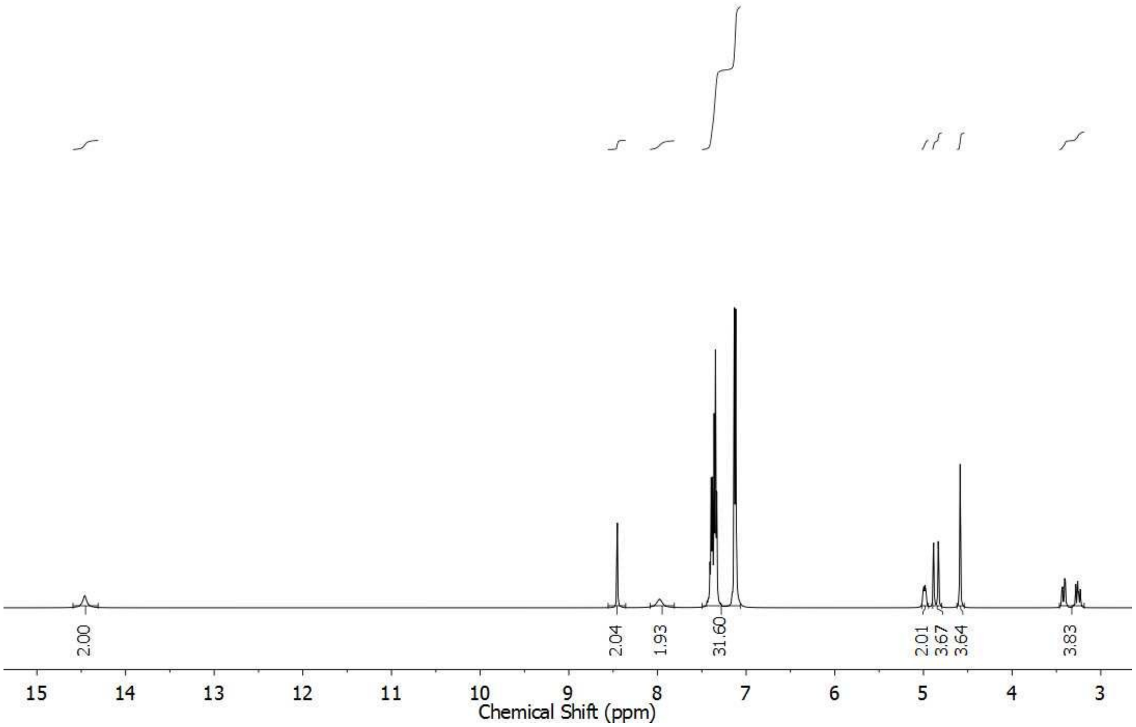

Figure S5. ^{1}H NMR spectrum of Fc[CO-His(Trt)-OH]$_2$ (**2**)

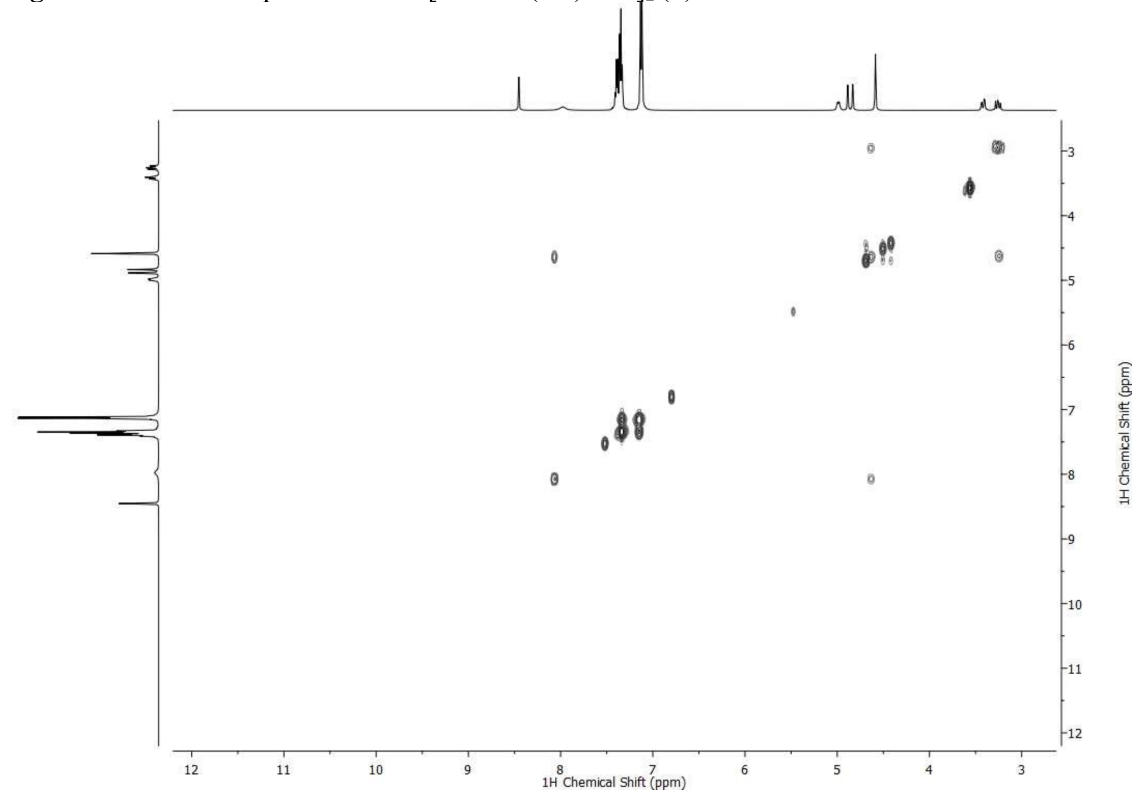

Figure S6. Two-dimensional ^{1}H-^{1}H gCOSY NMR spectrum of Fc[CO-His(Trt)-OH]$_2$ (**2**)

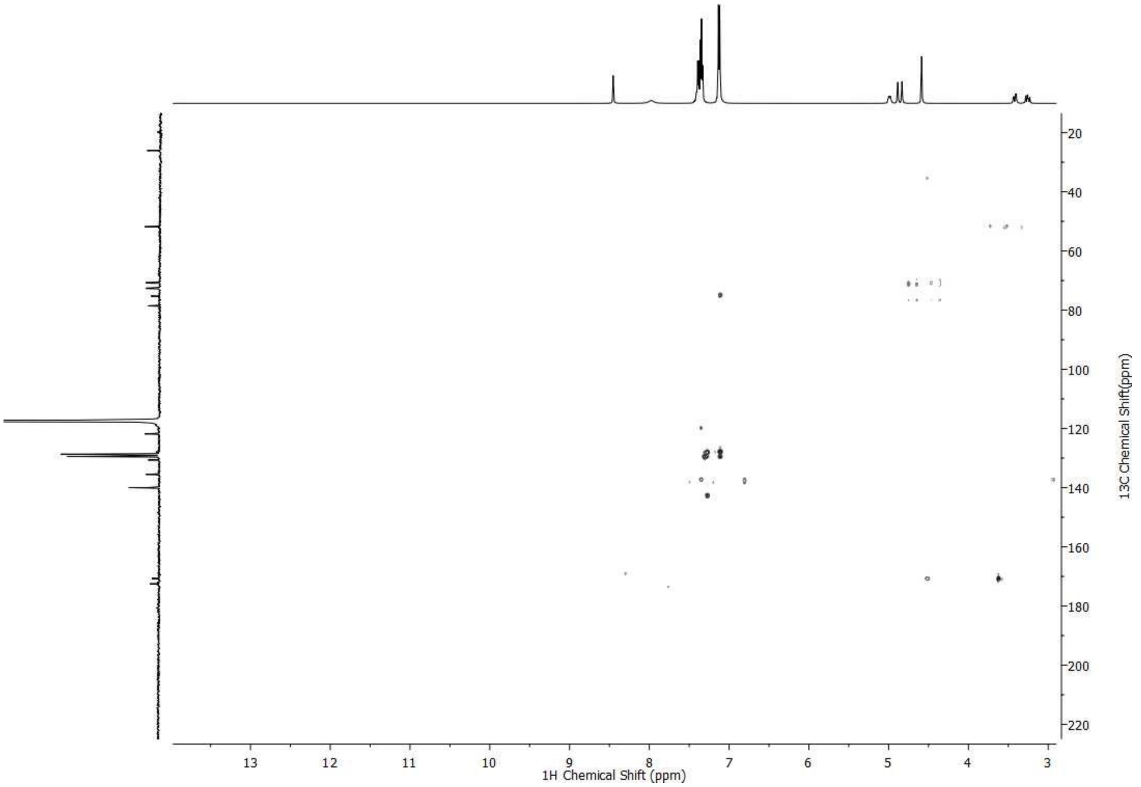

Figure S7. Two-dimensional gHMBCAD NMR spectrum of Fc[CO-His(Trt)-OH]$_2$ (**2**)

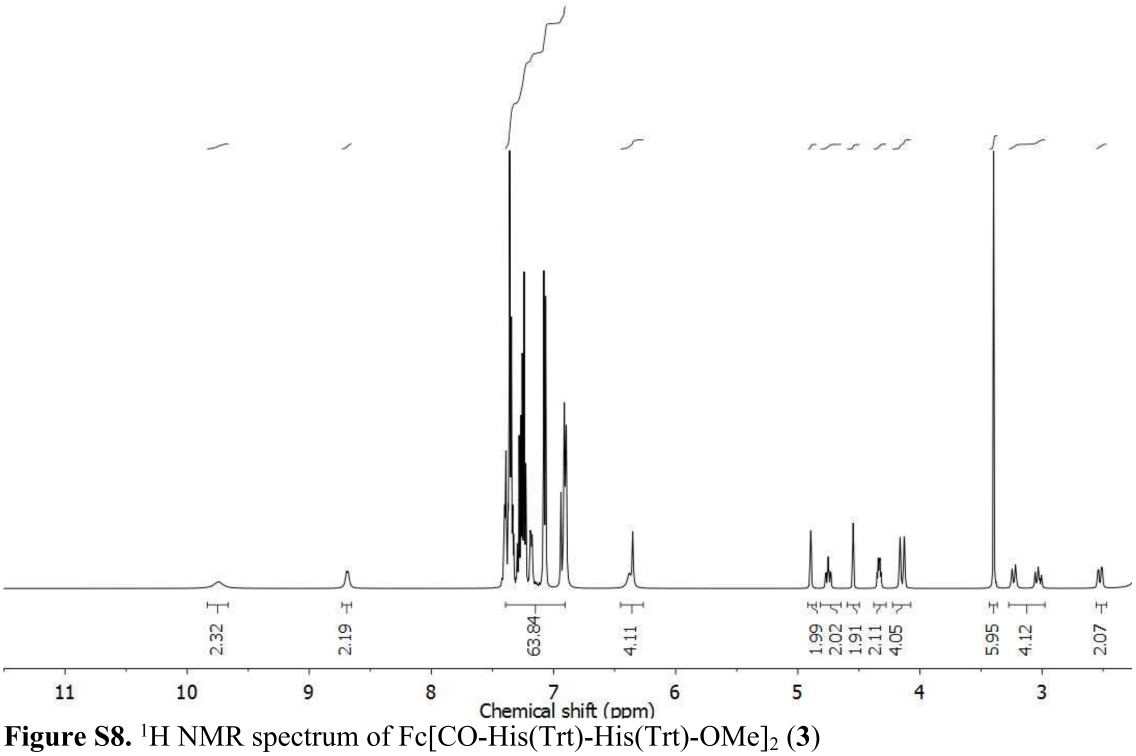

Figure S8. ^{1}H NMR spectrum of Fc[CO-His(Trt)-His(Trt)-OMe]$_2$ (**3**)

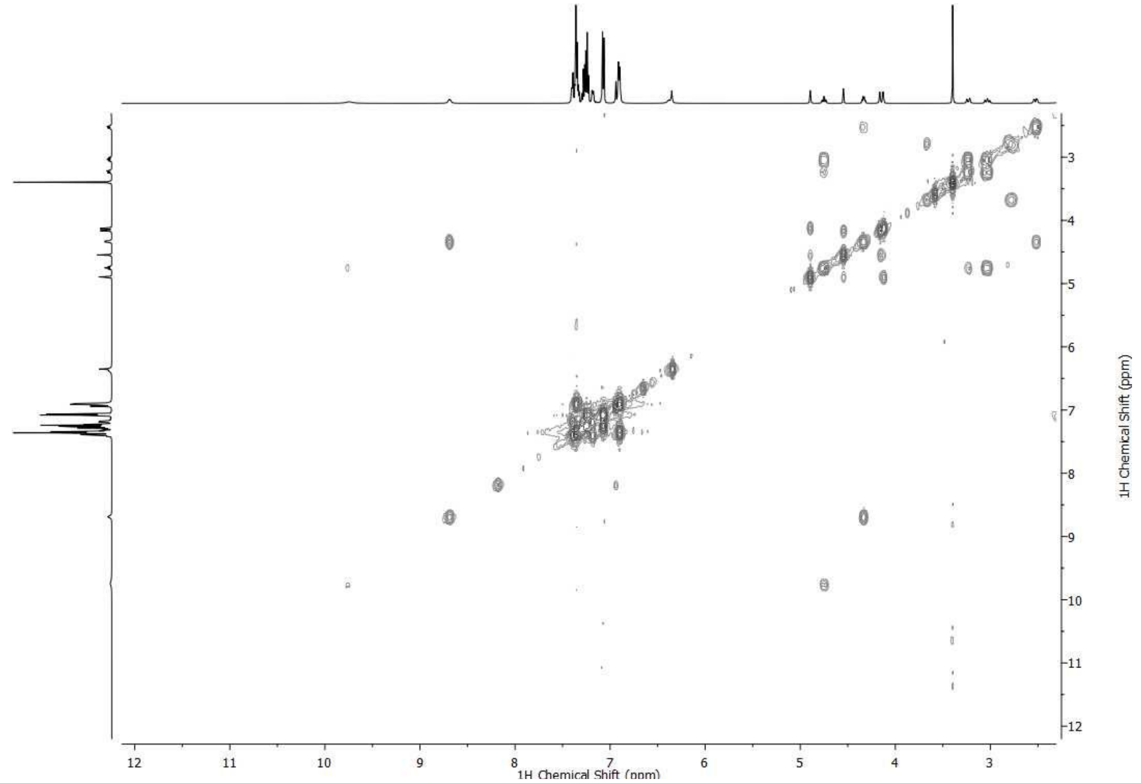

Figure S9. Two-dimensional ^{1}H-^{1}H gCOSY NMR spectrum of Fc[CO-His(Trt)-His(Trt)-OMe]$_2$ (**3**)

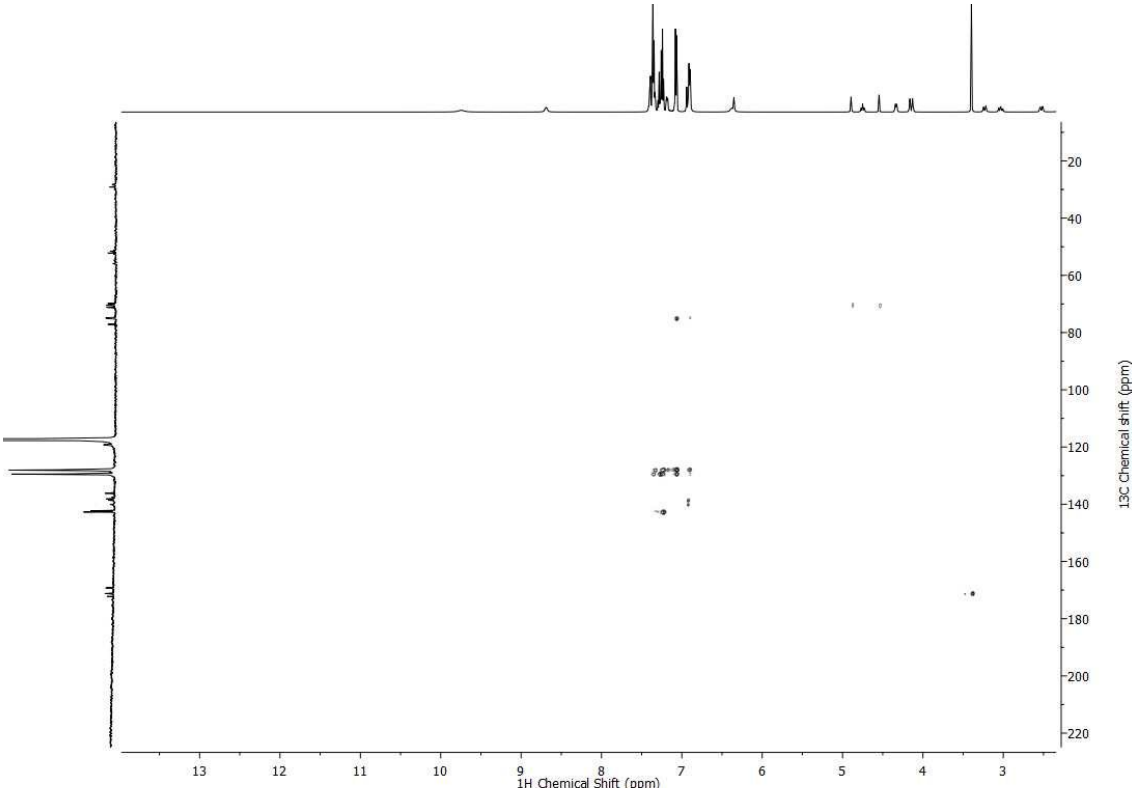

Figure S10. Two-dimensional gHMBCAD NMR spectrum of Fc[CO-His(Trt)-His(Trt)-OMe]$_2$ (**3**)

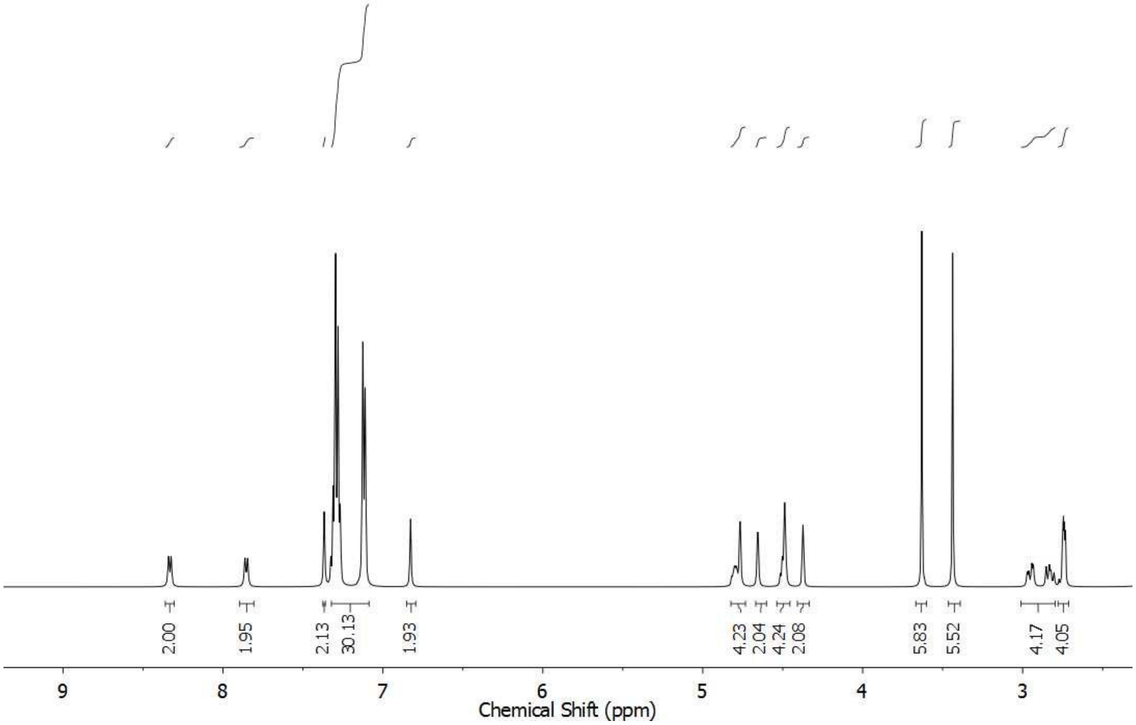

Figure S11. ^{1}H NMR spectrum of Fc[CO-His(Trt)-Asp(OMe)-OMe]$_2$ (**4**)

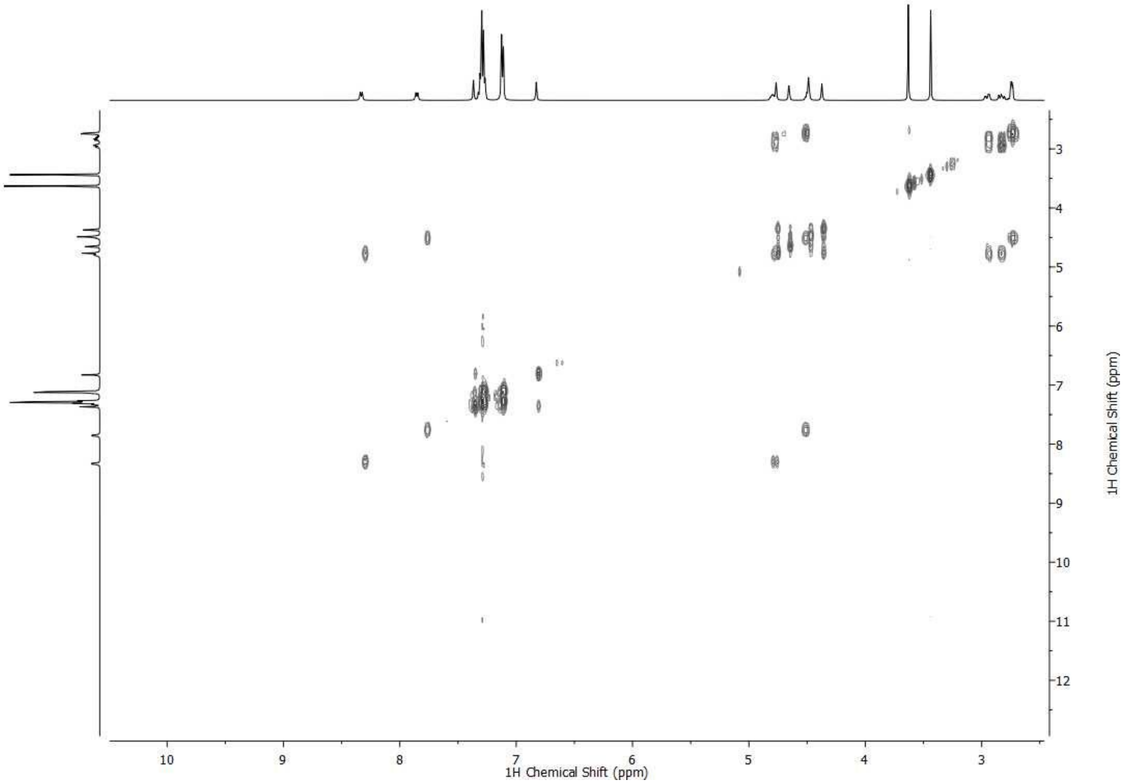

Figure S12. Two-dimensional ^{1}H-^{1}H gCOSY NMR spectrum of Fc[CO-His(Trt)-Asp(OMe)-OMe]$_2$ (**4**)

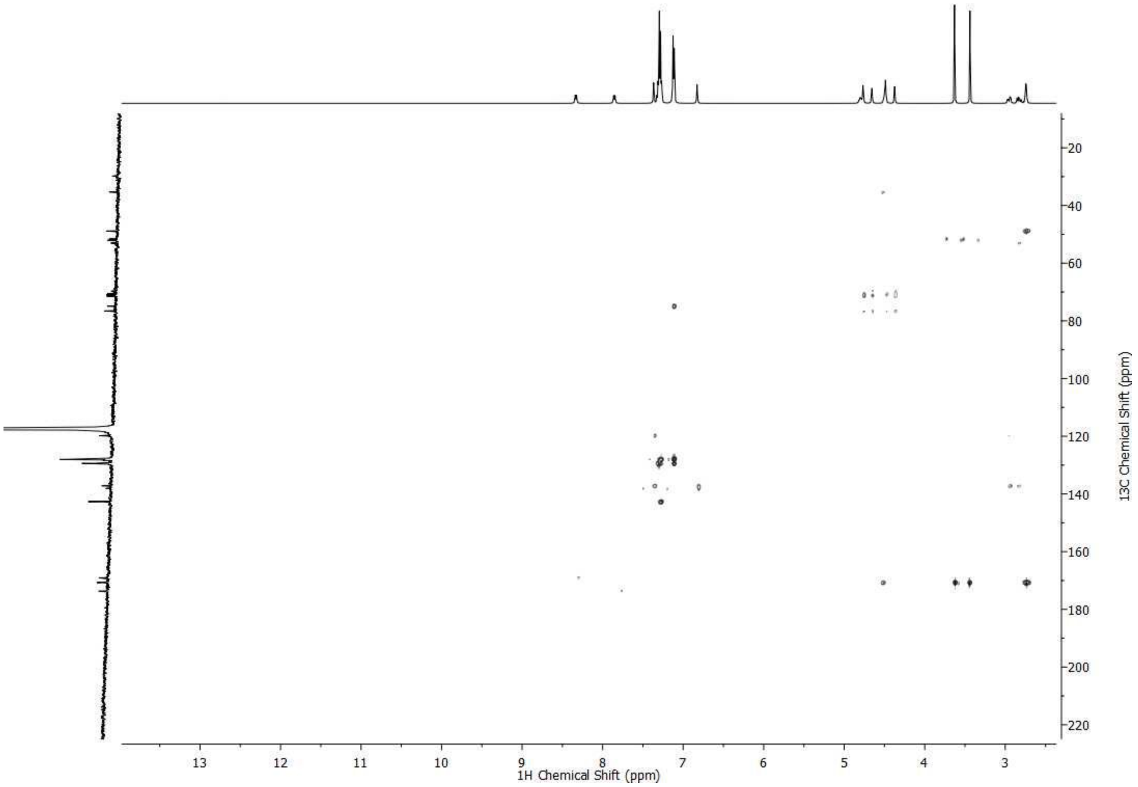

Figure S13. Two-dimensional gHMBCAD NMR spectrum of Fc[CO-His(Trt)-Asp(OMe)-OMe]$_2$ (**4**)

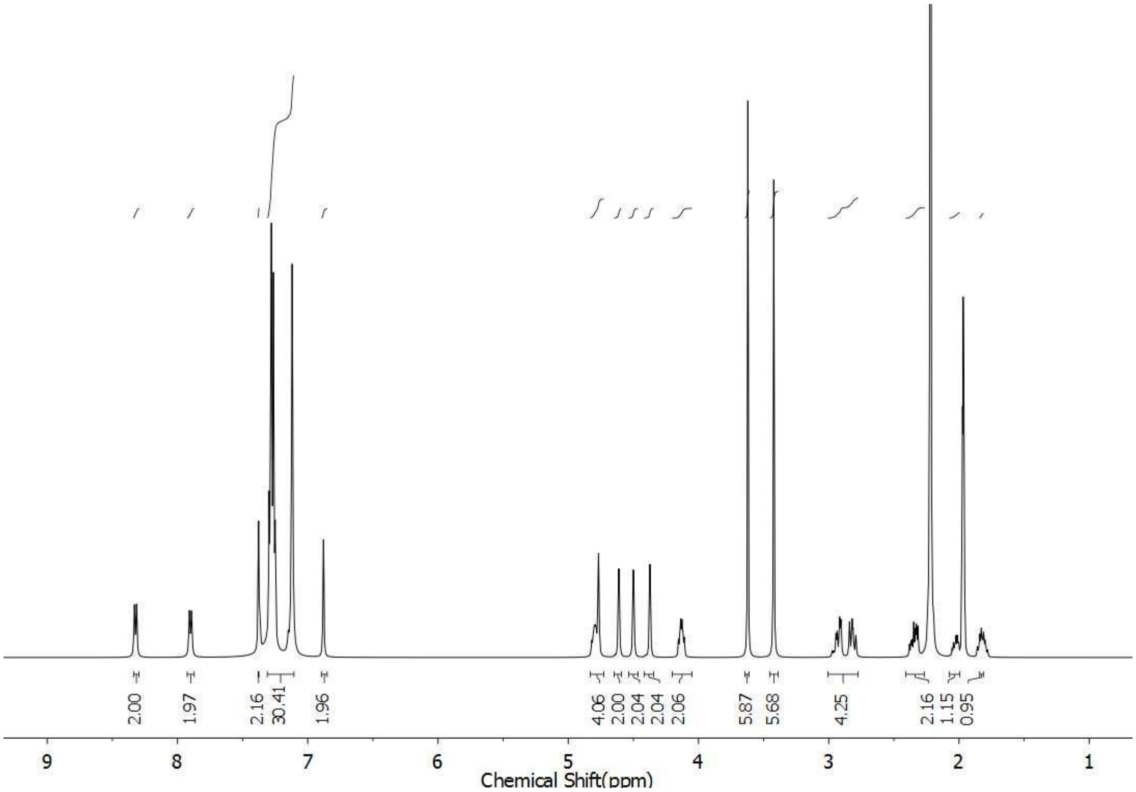

Figure S14. ^{1}H NMR spectrum of Fc[CO-His(Trt)-Glu(OMe)-OMe]$_2$ (**5**)

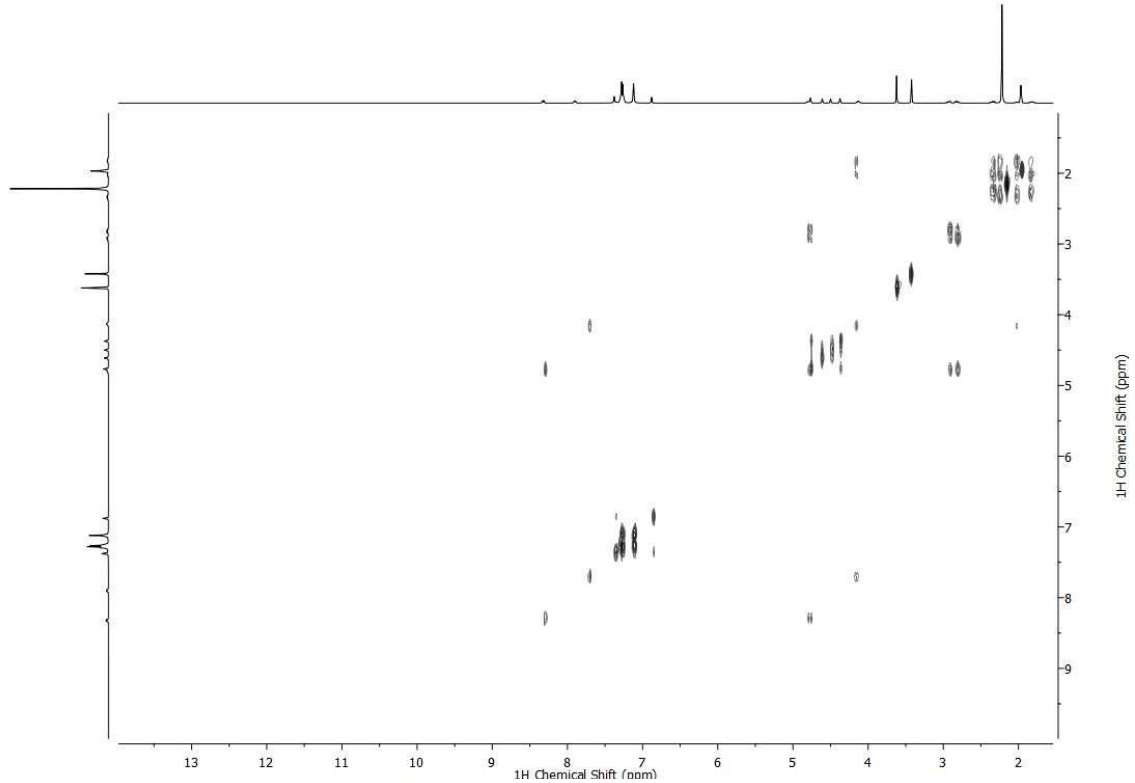

Figure S15. Two-dimensional ^1H-^1H gCOSY NMR spectrum of Fc[CO-His(Trt)-Glu(OMe)-OMe]$_2$ (**5**)

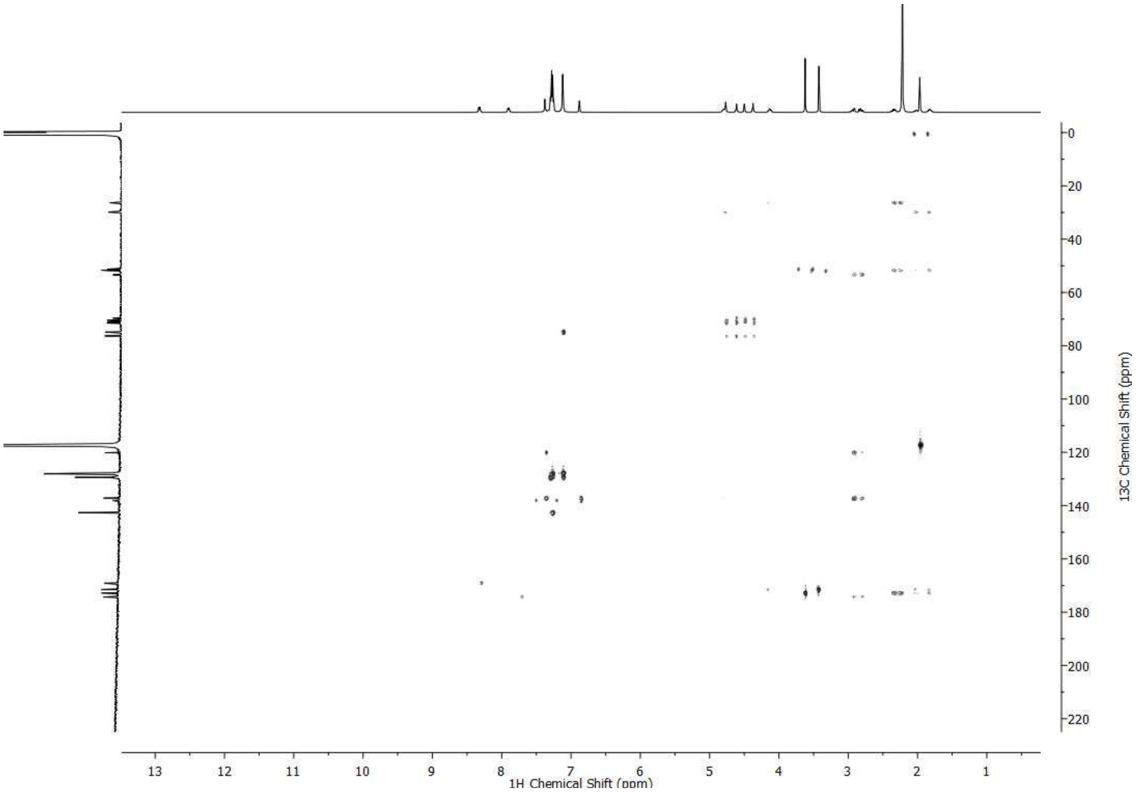

Figure S16. Two-dimensional gHMBCAD NMR spectrum of Fc[CO-His(Trt)-Glu(OMe)-OMe]$_2$ (**5**)

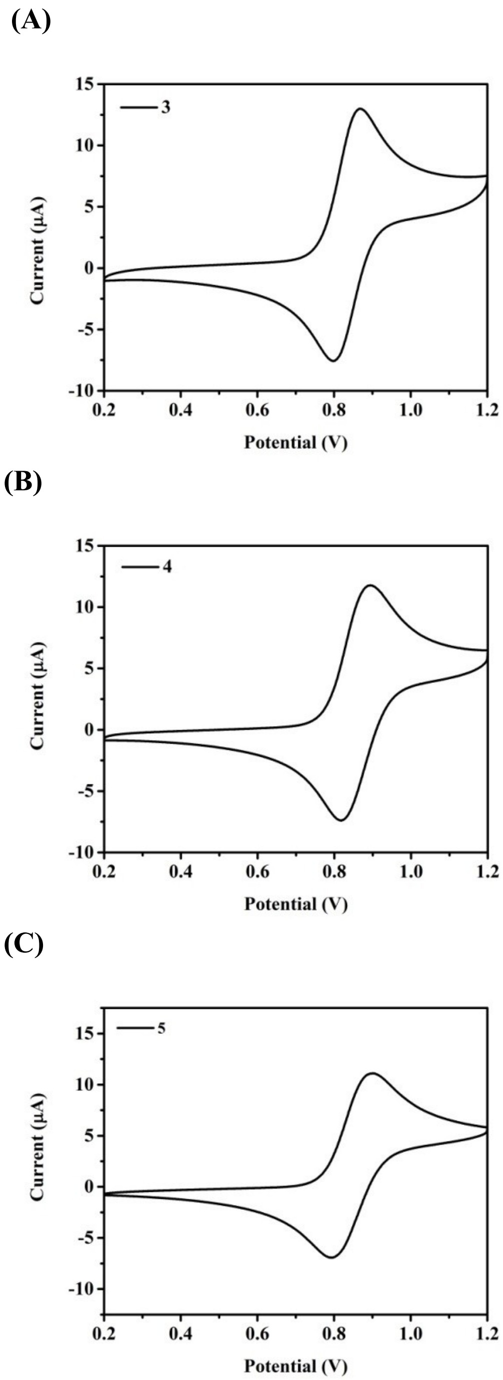

Figure S17. Cyclic voltammetry of a 1 mM solution of Fc-conjugate **3**, **4** and **5** in 0.1 M tetrabutylammonium perchlorate (TBAP) in acetonitrile at a scan rate of 100 mVs^{-1} are shown in **(A)**, **(B)**, and **(C)** for Fc-conjugate **3**, **4** and **5**, respectively. A 1 mM solution of ferrocene was recorded under identical conditions and referenced to Ag/AgCl. Glassy carbon working electrode and Pt wire counter electrode.

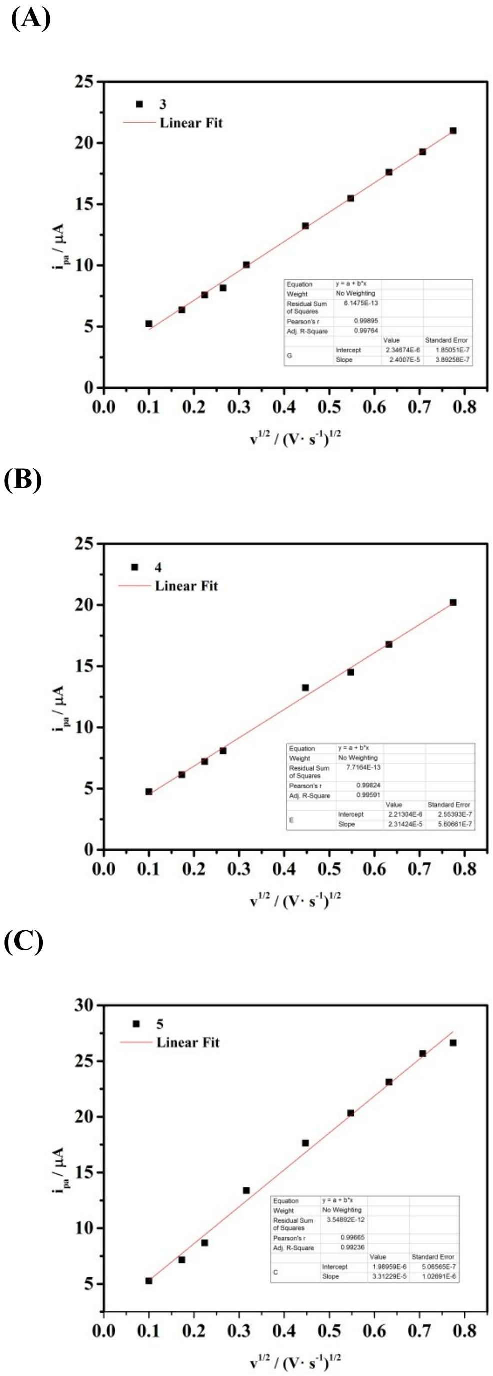

Equation	y = a + b*x		
Weight	No Weighting		
Residual Sum of Squares	6.1475E-13		
Pearson's r	0.99895		
Adj. R-Square	0.99764		
		Value	Standard Error
G	Intercept	2.34674E-6	1.85051E-7
	Slope	2.4007E-5	3.89258E-7

Equation	y = a + b*x		
Weight	No Weighting		
Residual Sum of Squares	7.7164E-13		
Pearson's r	0.99824		
Adj. R-Square	0.99591		
		Value	Standard Error
E	Intercept	2.21304E-6	2.55393E-7
	Slope	2.31424E-5	5.60661E-7

Equation	y = a + b*x		
Weight	No Weighting		
Residual Sum of Squares	3.54892E-12		
Pearson's r	0.99665		
Adj. R-Square	0.99236		
		Value	Standard Error
C	Intercept	1.98959E-6	5.06565E-7
	Slope	3.31229E-5	1.02691E-6

Figure S18. The peak current function $i_{pa}/n^{1/2}$ (n = scan rate) are shown **(A)**, **(B)**, and **(C)** for Fc-conjugate **3**, **4** and **5**, respectively. Variable scan rate experiments were carried out in a range from 10-600 mV s^{-1}.

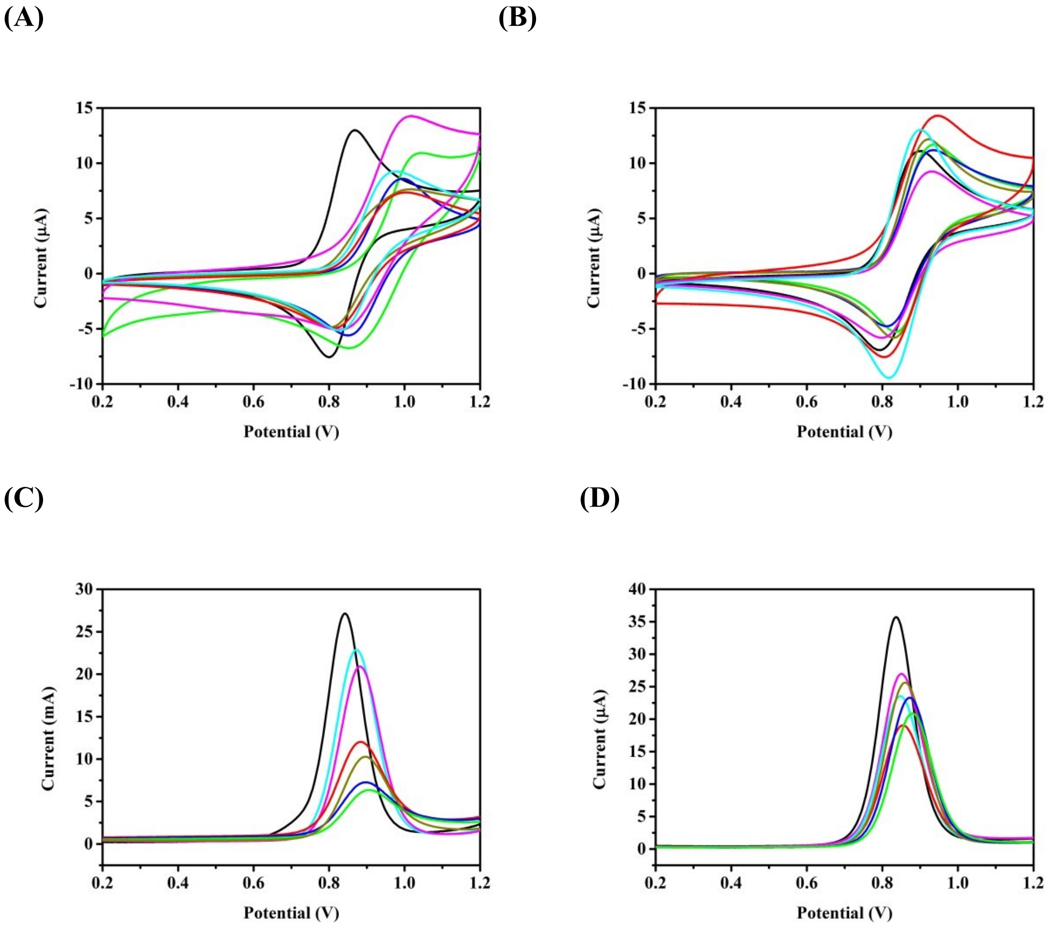

Figure S19. Cyclic voltammograms of Fc-conjugate **3 (A), 5 (B)** and square wave voltammogram of Fc-peptide **3 (C)** and **5 (D)** in acetonitrile are shown before (black solid lines) and after addition of 3 equiv. of different metal ions: Mg^{2+} (cyan), Mn^{2+} (magenta), Cu^{2+} (green), Zn^{2+} (blue), Ni^{2+} (dark yellow), and Cd^{2+} (red). The addition of metal perchlorate salts caused anodic shifts ([Fc-conjugate **3** and **5**] = 1 mM, acetonitrile, 0.1 M TBAP was added as supporting electrolyte; glassy carbon working electrode, Pt wire counter electrode, Ag/AgCl reference electrode).

(A)

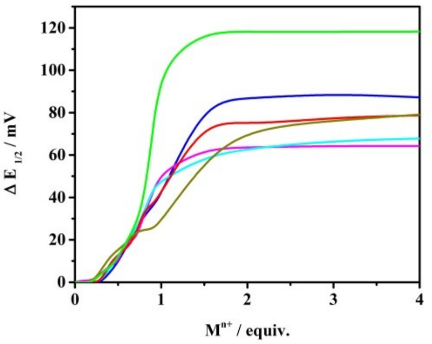

(B)

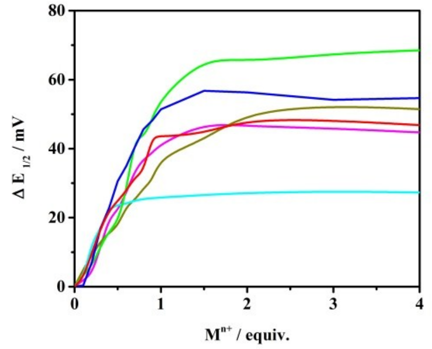

(C)

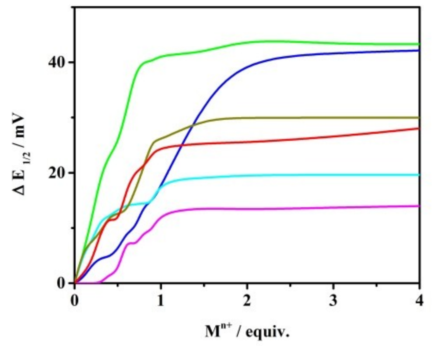

Figure S20. Effects of metal ion addition on the half-wave potential of compound **3 (A)**, **4 (B)** and **5 (C)** (1 mM in acetonitrile). The following metal ions were added as their perchlorate salts: Mg^{2+} (cyan), Mn^{2+} (magenta), Cu^{2+} (green), Zn^{2+} (blue), Ni^{2+} (dark yellow), and Cd^{2+} (red).

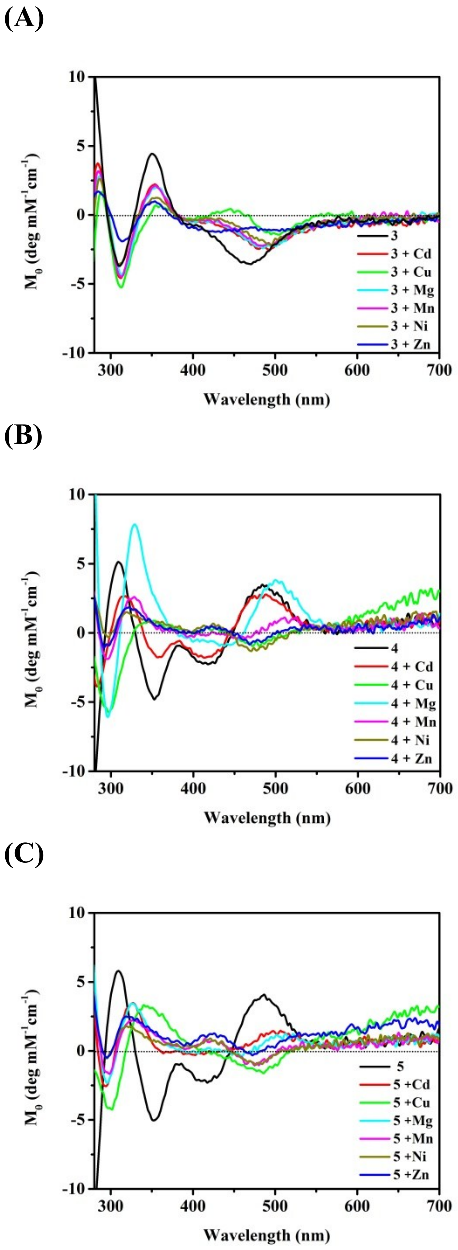

Figure S21. CD spectra of Fc-conjugate **3 (A)**, **4(B)** and **5 (C)** (in acetonitrile) before addition of 1 equiv. (black) of metal ions and after addition of different metal perchlorate salts: Mg^{2+} (cyan), Mn^{2+} (magenta), Cu^{2+} (green), Zn^{2+} (blue), Ni^{2+} (dark yellow), and Cd^{2+} (red).

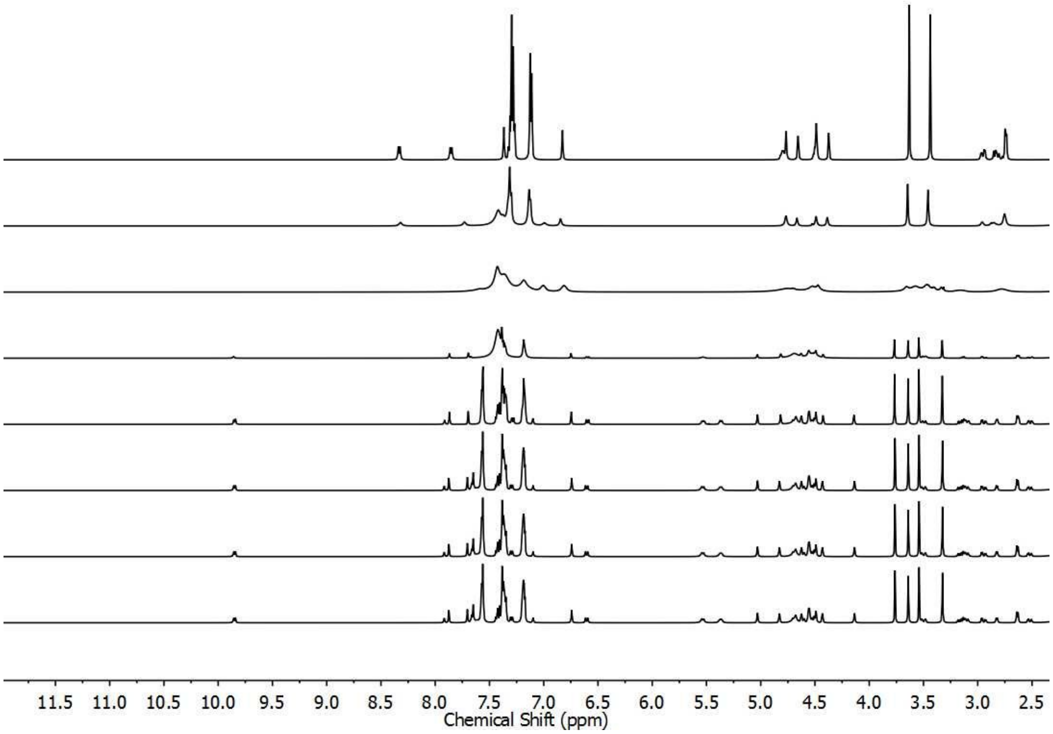

Figure S22. ^{1}H NMR spectroscopic titration experiments of Cd^{2+}. Cd^{2+} was added at 0, 0.2, 0.4, 0.6, 1.0, 1.2, 1.4 and 2.0 equiv. shown from top to bottom ([Fc-conjugate **4**] = 1mM, CD_3CN)

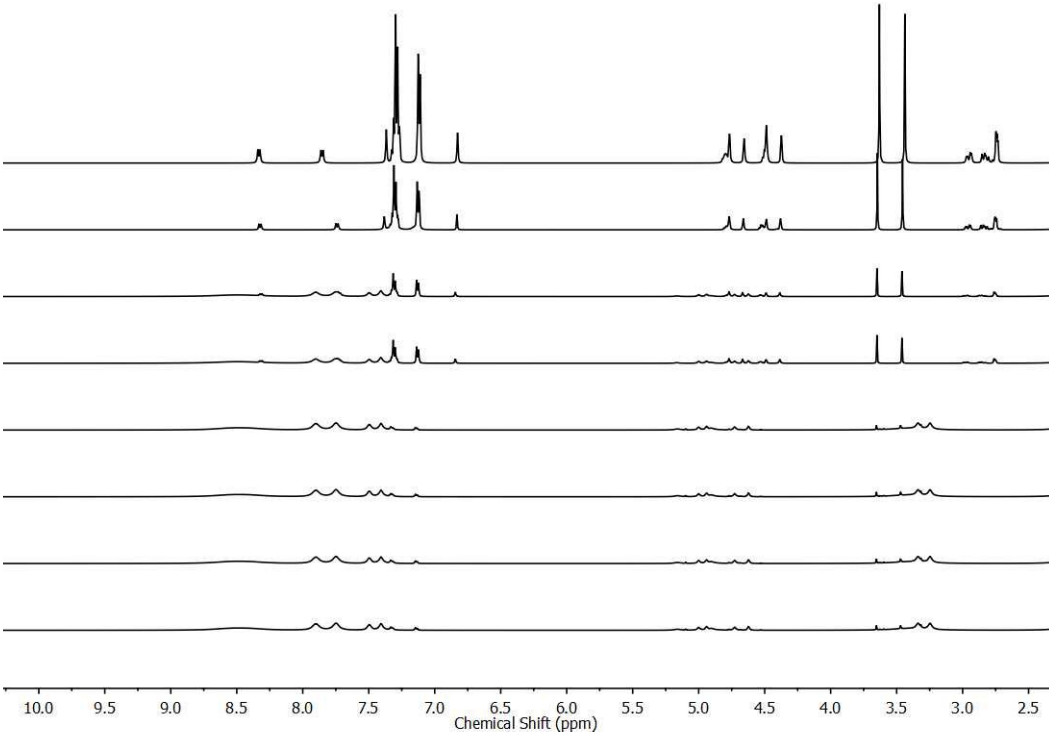

Figure S23. ^{1}H NMR spectroscopic titration experiments of Ni^{2+}. Ni^{2+} was added at at 0, 0.2, 0.4, 0.6, 1.0, 1.2, 1.4 and 2.0 equiv. shown from top to bottom ([Fc-conjugate **4**] = 1mM, CD_3CN)

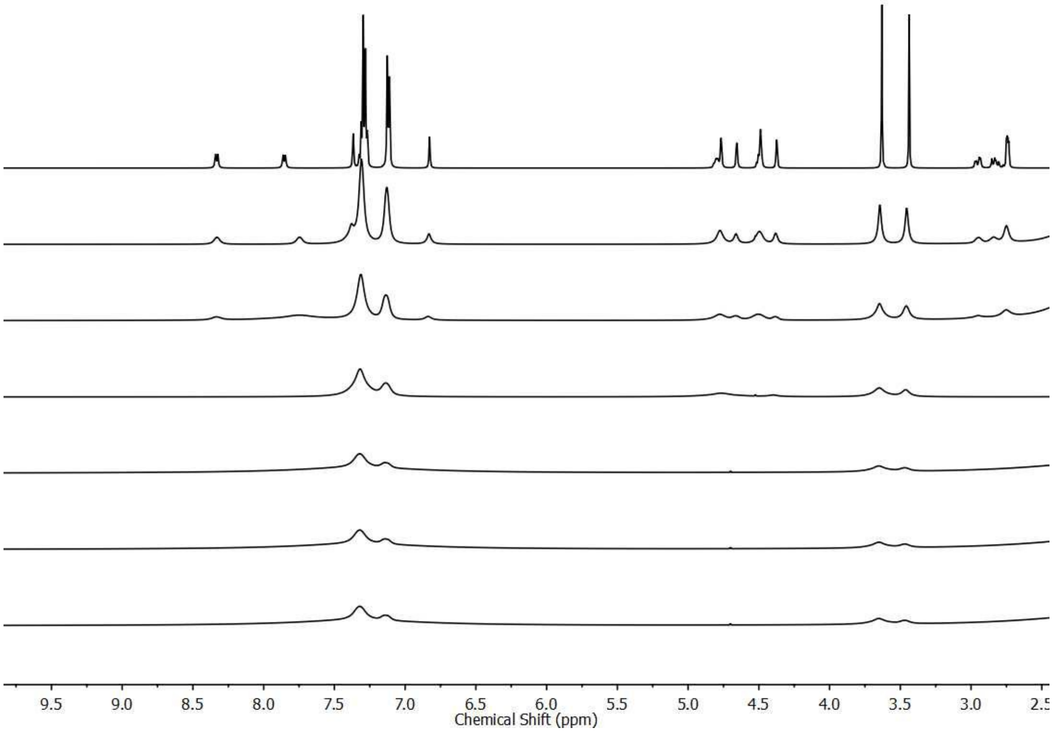

Figure S24. ^{1}H NMR spectroscopic titration experiments of Mn^{2+}. Mn^{2+} was added at at 0, 0.2, 0.4, 0.6, 1.0, 1.2, 1.4 and 2.0 equiv. shown from top to bottom ([Fc-conjugate **4**] = 1mM, CD_3CN)

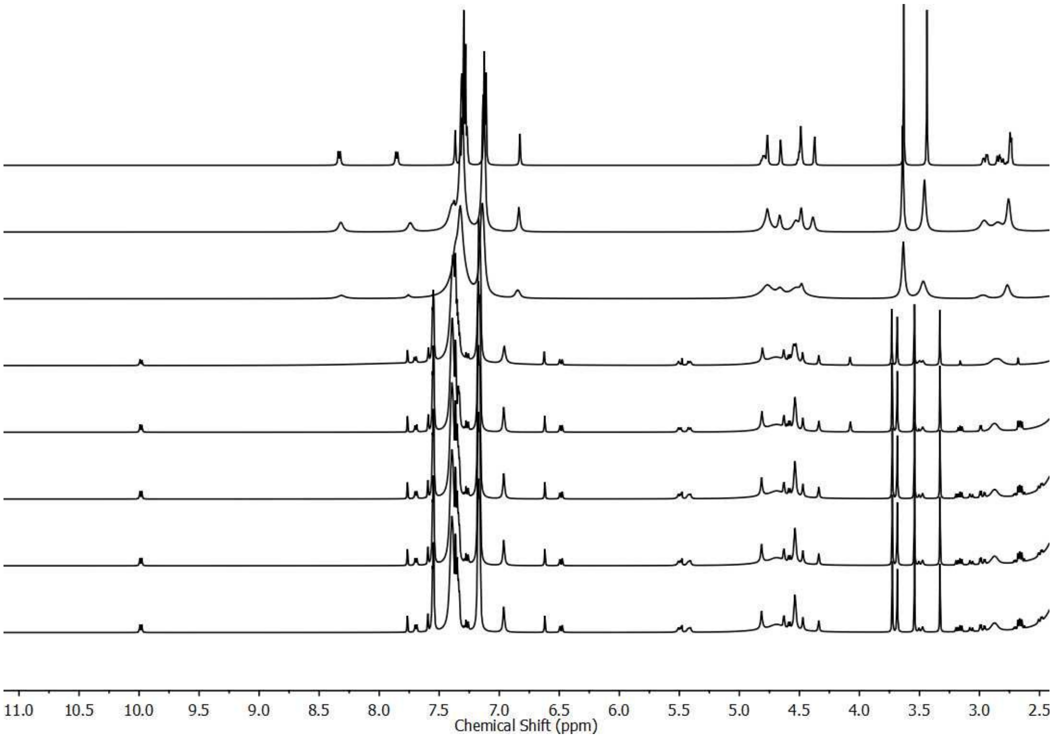

Figure S25. ^{1}H NMR spectroscopic titration experiments of Mg^{2+}. Mg^{2+} was added at at 0, 0.2, 0.4, 0.6, 1.0, 1.2, 1.4 and 2.0 equiv. shown from top to bottom ([Fc-conjugate **4**] = 1mM, CD_3CN)

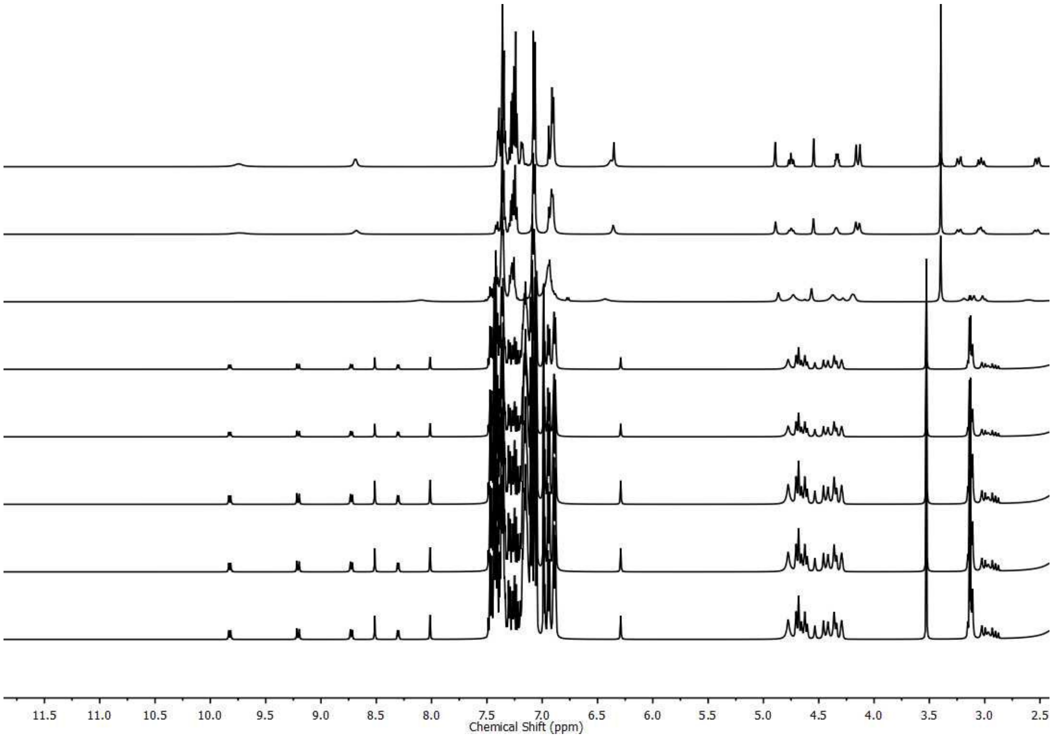

Figure S26. ^{1}H NMR spectroscopic titration experiments of Zn^{2+}. Zn^{2+} was added at at 0, 0.2, 0.4, 0.6, 1.0, 1.2, 1.4 and 2.0 equiv. shown from top to bottom ([Fc-conjugate **3**] = 1mM, CD_3CN)

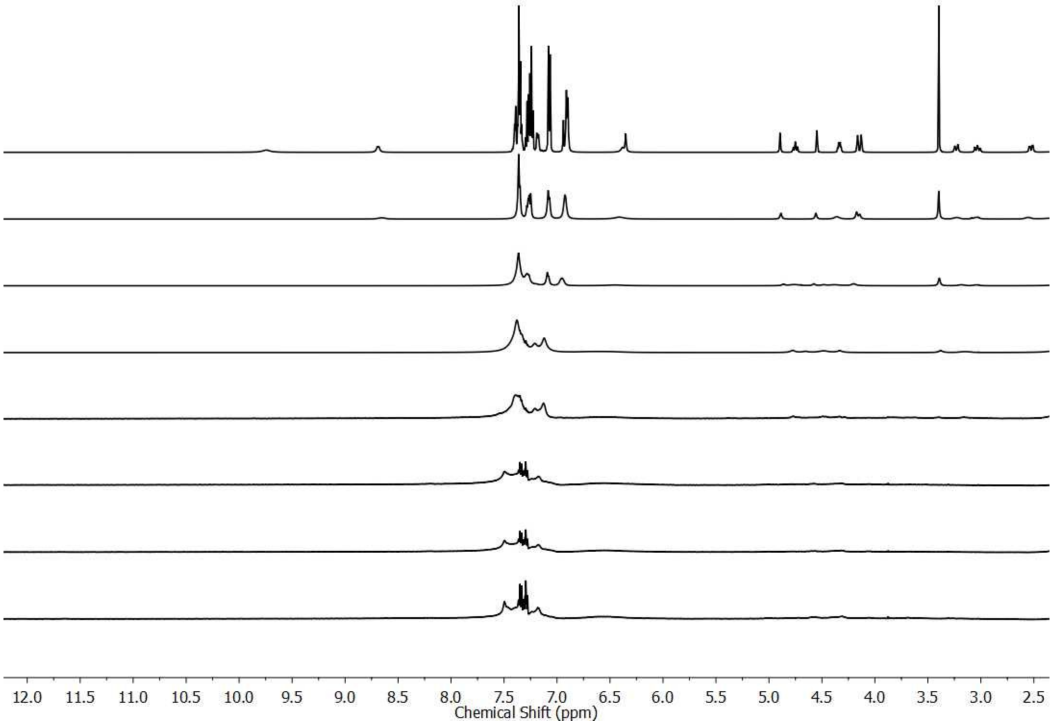

Figure S27. ^{1}H NMR spectroscopic titration experiments of Cu^{2+}. Cu^{2+} was added at at 0, 0.2, 0.4, 0.6, 1.0, 1.2, 1.4 and 2.0 equiv. shown from top to bottom ([Fc-conjugate **3**] = 1mM, CD_3CN)

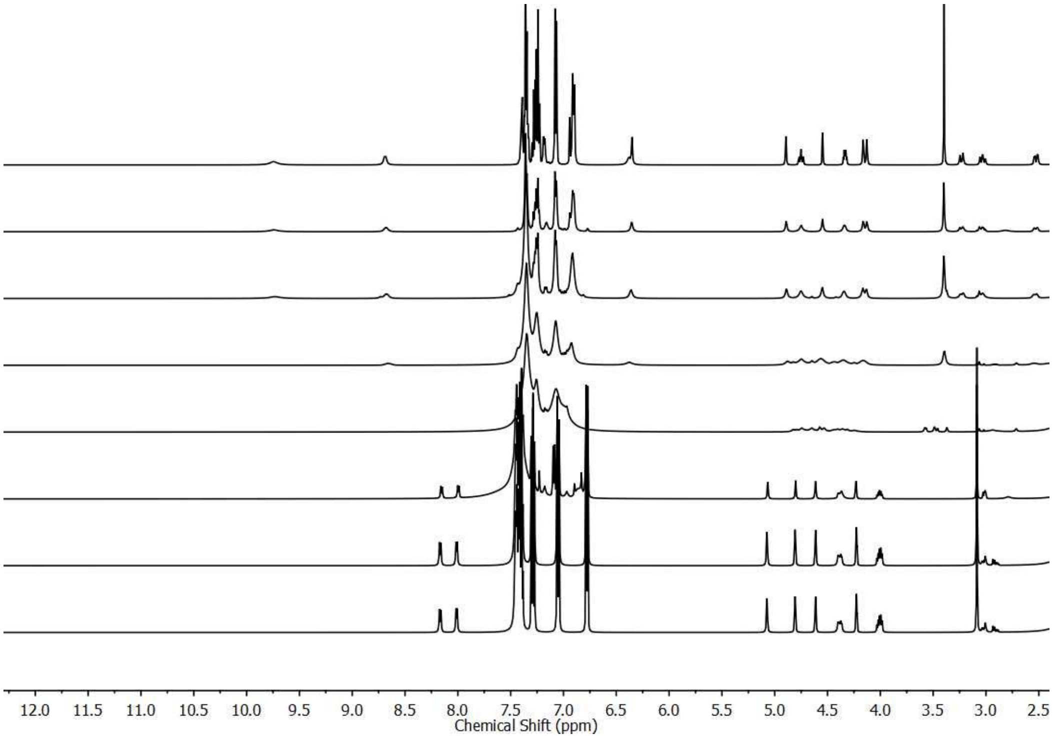

Figure S28. ^{1}H NMR spectroscopic titration experiments of Cd^{2+}. Cd^{2+} was added at at 0, 0.2, 0.4, 0.6, 1.0, 1.2, 1.4 and 2.0 equiv. shown from top to bottom ([Fc-conjugate **3**] = 1mM, CD_3CN)

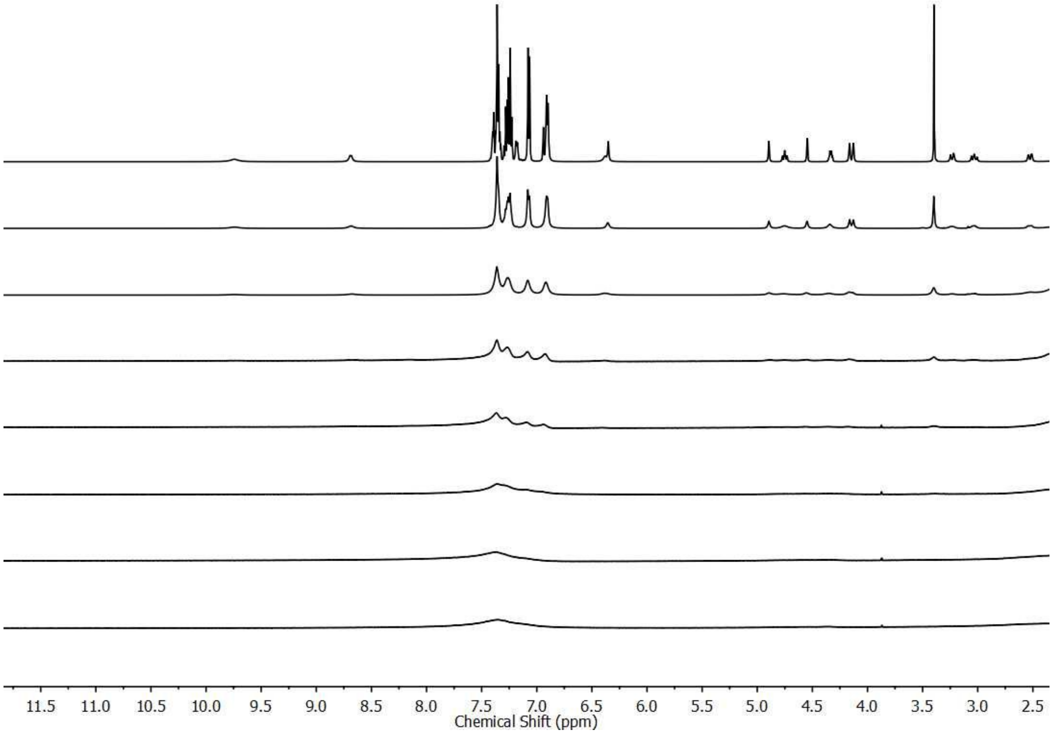

Figure S29. ^{1}H NMR spectroscopic titration experiments of Mn^{2+}. Mn^{2+} was added at at 0, 0.2, 0.4, 0.6, 1.0, 1.2, 1.4 and 2.0 equiv. shown from top to bottom ([Fc-conjugate **3**] = 1mM, CD_3CN)

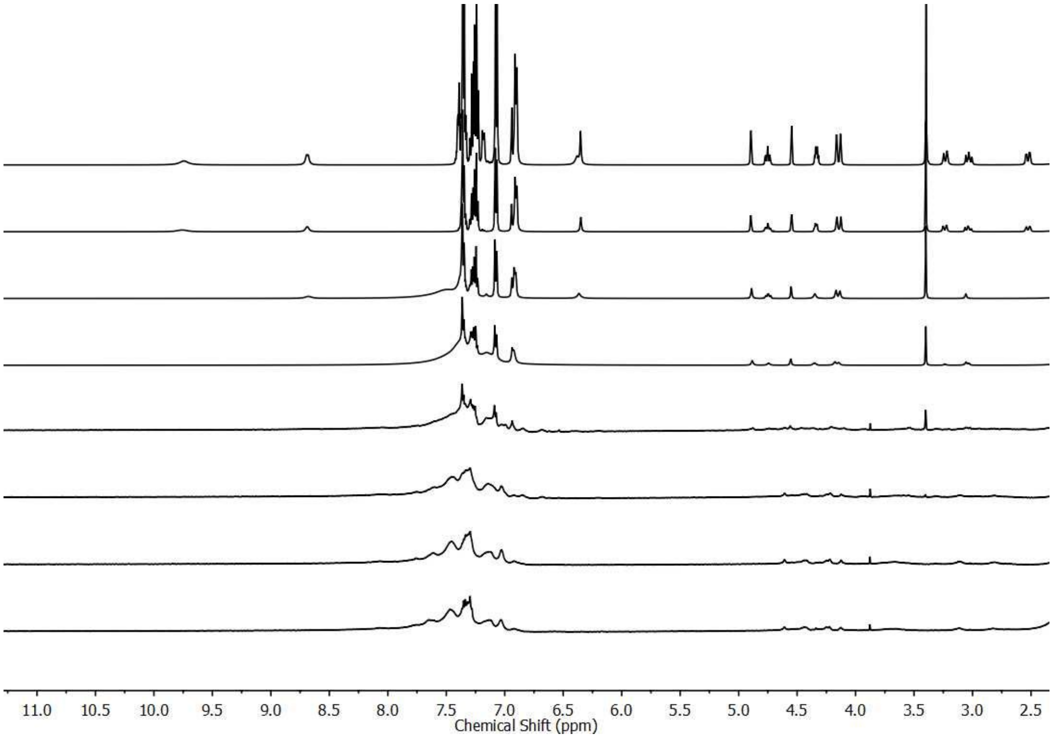

Figure S30. ^{1}H NMR spectroscopic titration experiments of Ni^{2+}. Ni^{2+} was added at 0, 0.2, 0.4, 0.6, 1.0, 1.2, 1.4 and 2.0 equiv. shown from top to bottom ([Fc-conjugate **3**] = 1mM, CD_3CN)

Figure S31. ^{1}H NMR spectroscopic titration experiments of Mg^{2+}. Mg^{2+} was added at at 0, 0.2, 0.4, 0.6, 1.0, 1.2, 1.4 and 2.0 equiv. shown from top to bottom ([Fc-conjugate **3**] = 1mM, CD_3CN)

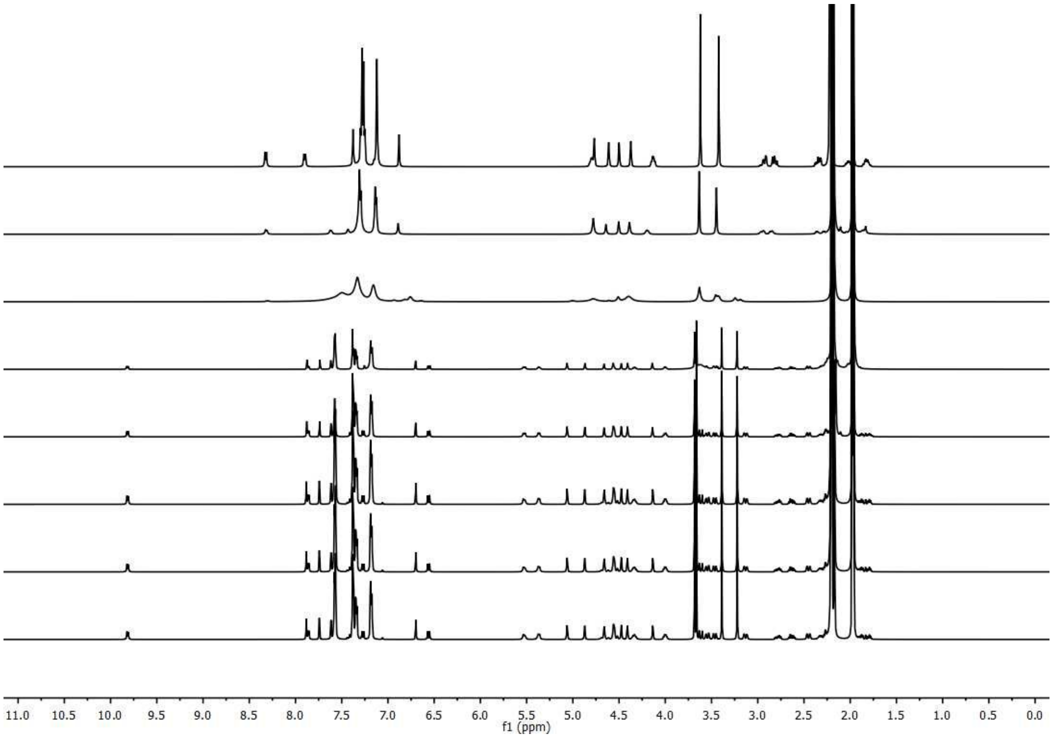

Figure S32. ^{1}H NMR spectroscopic titration experiments of Zn^{2+}. Zn^{2+} was added at at 0, 0.2, 0.4, 0.6, 1.0, 1.2, 1.4 and 2.0 equiv. shown from top to bottom ([Fc-conjugate **5**] = 1mM, CD_3CN)

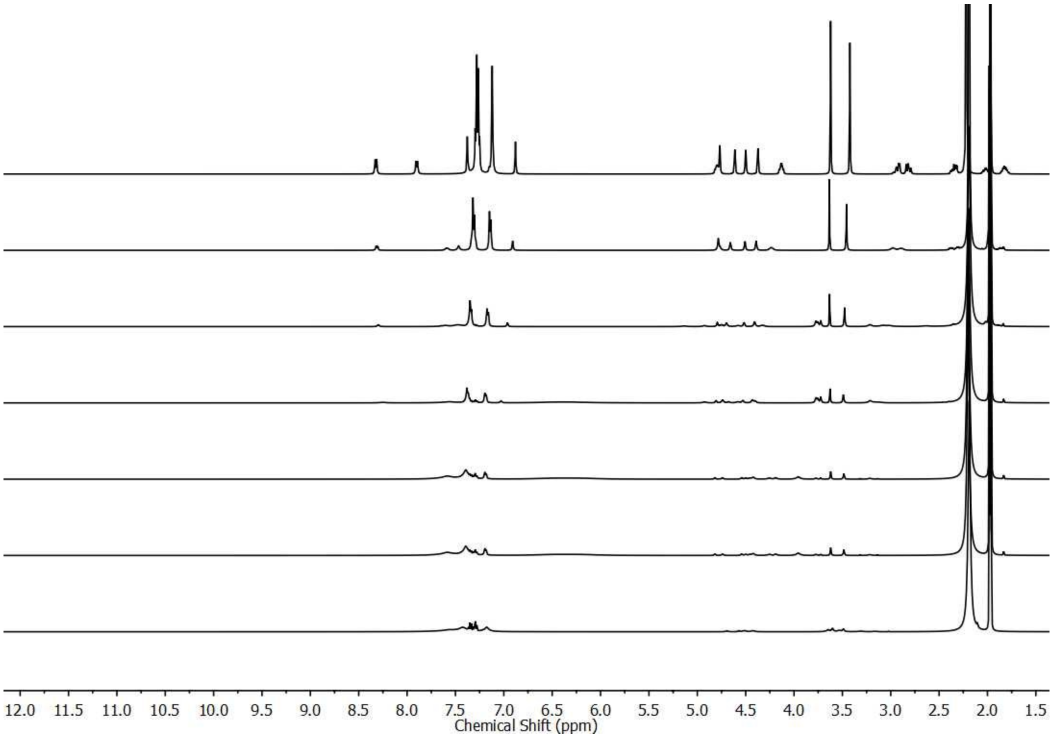

Figure S33. ^{1}H NMR spectroscopic titration experiments of Cu^{2+}. Cu^{2+} was added at at 0, 0.2, 0.4, 0.6, 1.0, 1.2, 1.4 and 2.0 equiv. shown from top to bottom ([Fc-conjugate **5**] = 1mM, CD_3CN)

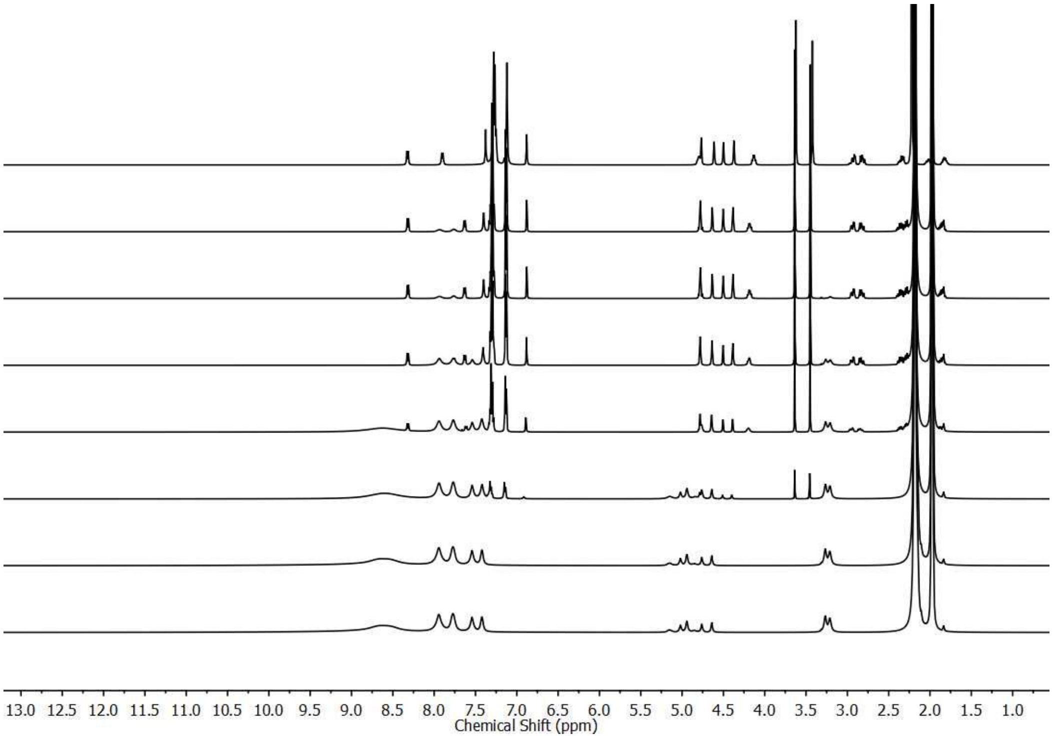

Figure S34. ^{1}H NMR spectroscopic titration experiments of Ni^{2+}. Ni^{2+} was added at at 0, 0.2, 0.4, 0.6, 1.0, 1.2, 1.4 and 2.0 equiv. shown from top to bottom ([Fc-conjugate **5**] = 1mM, CD_3CN)

Figure S35. ^{1}H NMR spectroscopic titration experiments of Cd^{2+}. Cd^{2+} was added at at 0, 0.2, 0.4, 0.6, 1.0, 1.2, 1.4 and 2.0 equiv. shown from top to bottom ([Fc-conjugate **5**] = 1mM, CD_3CN)

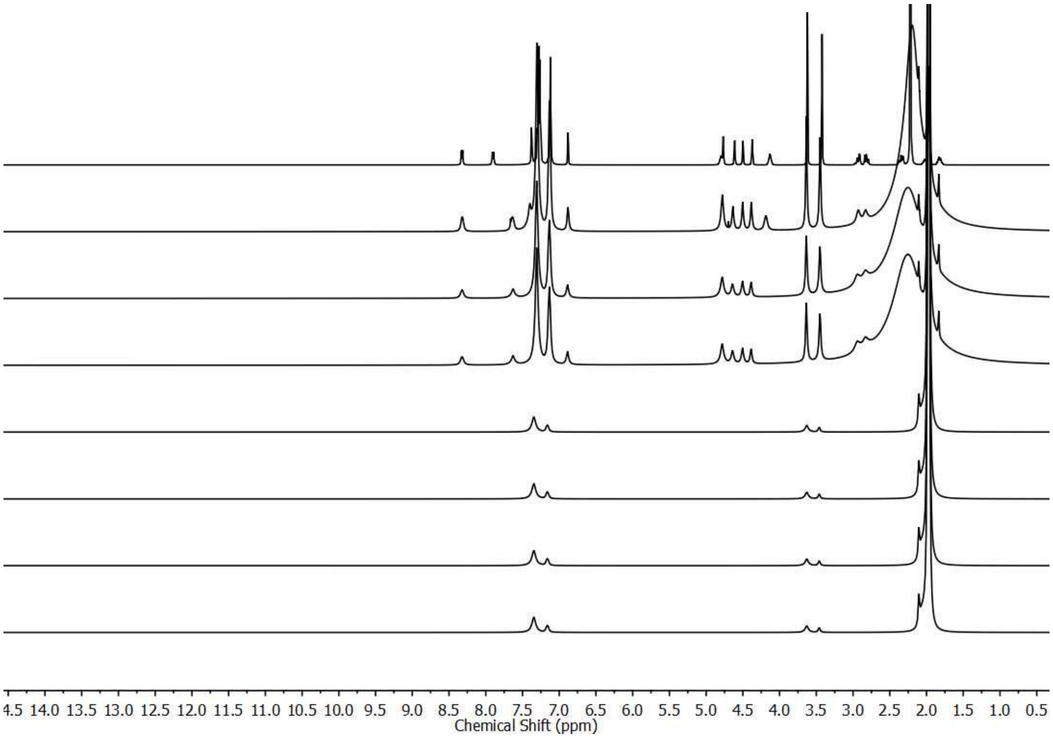

Figure S36. ^{1}H NMR spectroscopic titration experiments of Mn^{2+}. Mn^{2+} was added at 0, 0.2, 0.4, 0.6, 1.0, 1.2, 1.4 and 2.0 equiv. shown from top to bottom ([Fc-conjugate **5**] = 1mM, CD_3CN)

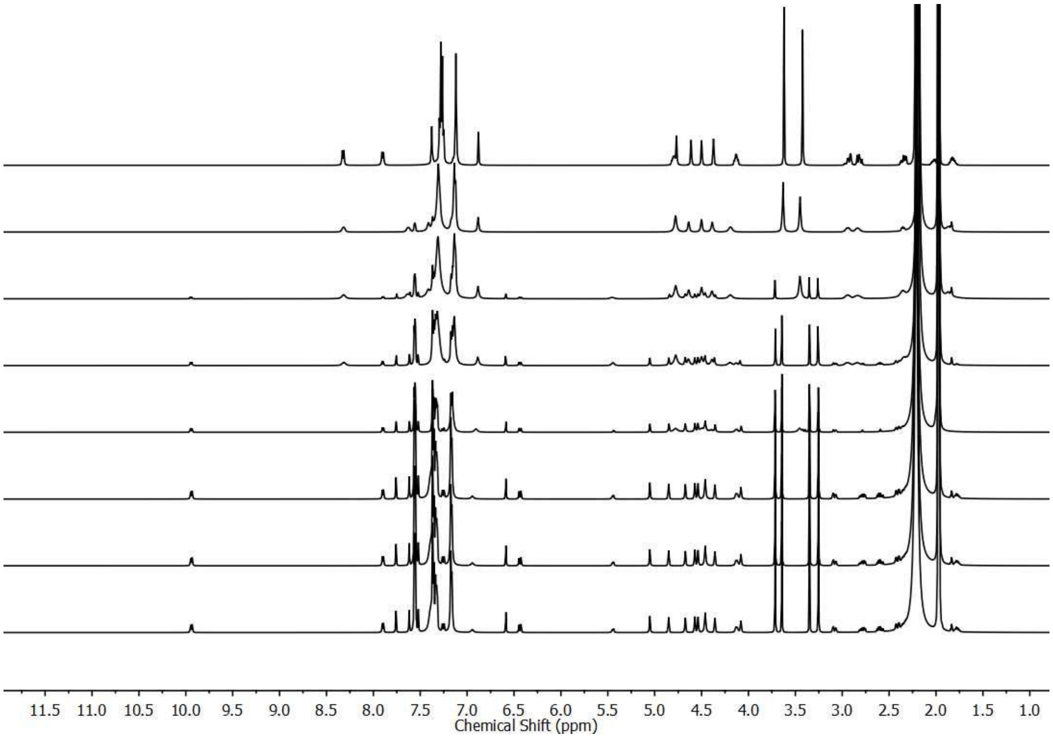

Figure S37. ^{1}H NMR spectroscopic titration experiments of Mg^{2+}. Mg^{2+} was added at at 0, 0.2, 0.4, 0.6, 1.0, 1.2, 1.4 and 2.0 equiv. shown from top to bottom ([Fc-conjugate **5**] = 1mM, CD_3CN)

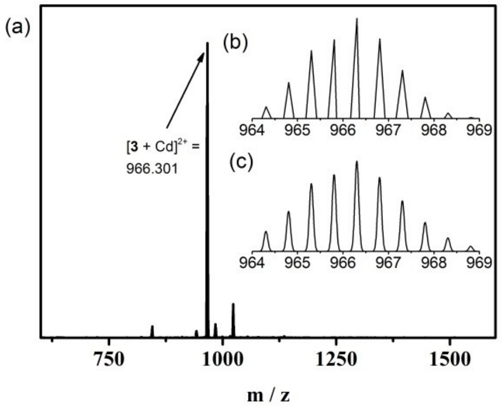

Figure S38. (a) The experimental ESI-MS+ (positive mode) results showing **3** in acetonitrile with the presence of Cd^{2+}. (b) Partial spectrum of the molecular ion of **3**·Cd with an overall of 2+ charge. (c) Theoretical isotopic pattern of the Cd^{2+} complexed to conjugate **3** assigned to [**3** + Cd]$^{2+}$.

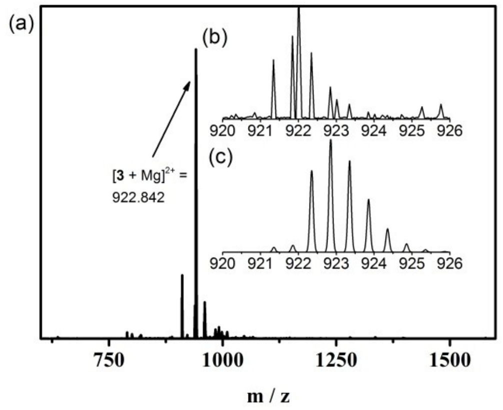

Figure S39. (a) The experimental ESI-MS+ (positive mode) results showing **3** in acetonitrile with the presence of Mg^{2+}. (b) Partial spectrum of the molecular ion of **3**·Mg with an overall of 2+ charge. (c) Theoretical isotopic pattern of the Mg^{2+} complexed to conjugate **3** assigned to [**3** + Mg]$^{2+}$.

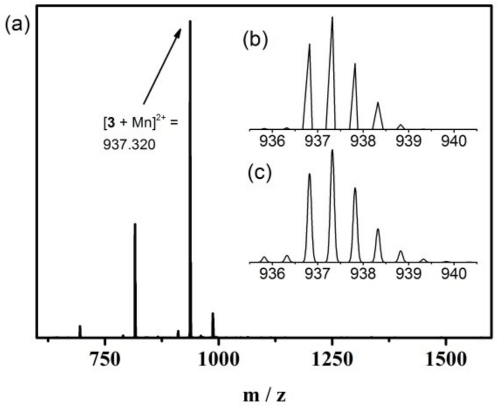

Figure S40. (a) The experimental ESI-MS+ (positive mode) results showing **3** in acetonitrile with the presence of Mn^{2+}. (b) Partial spectrum of the molecular ion of **3**·Mn with an overall of 2+ charge. (c) Theoretical isotopic pattern of the Mn^{2+} complexed to conjugate **3** assigned to [**3** + Mn]$^{2+}$.

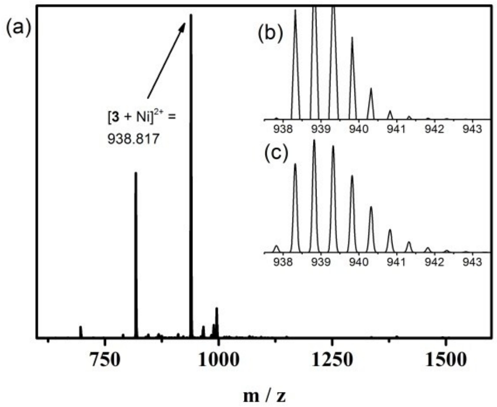

Figure S41. (a) The experimental ESI-MS+ (positive mode) results showing **3** in acetonitrile with the presence of Ni^{2+}. (b) Partial spectrum of the molecular ion of **3**·Ni with an overall of 2+ charge. (c) Theoretical isotopic pattern of the Ni^{2+} complexed to conjugate **3** assigned to [**3** + Ni]$^{2+}$.

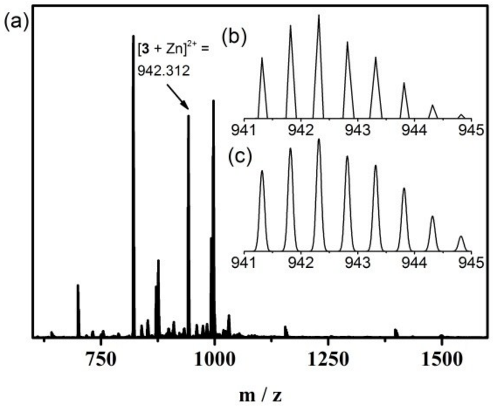

Figure S42. (a) The experimental ESI-MS+ (positive mode) results showing **3** in acetonitrile with the presence of Zn^{2+}. (b) Partial spectrum of the molecular ion of **3**·Zn with an overall of 2+ charge. (c) Theoretical isotopic pattern of the Zn^{2+} complexed to conjugate **3** assigned to [**3** + Zn]$^{2+}$.

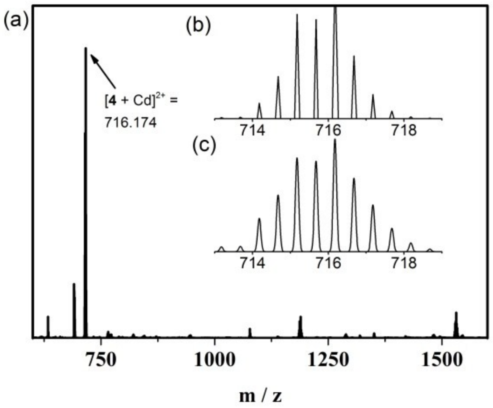

Figure S43. (a) The experimental ESI-MS+ (positive mode) results showing **4** in acetonitrile with the presence of Cd^{2+}. (b) Partial spectrum of the molecular ion of **4**·Cd with an overall of 2+ charge. (c) Theoretical isotopic pattern of the Cd^{2+} complexed to conjugate **4** assigned to [**4** + Cd]$^{2+}$.

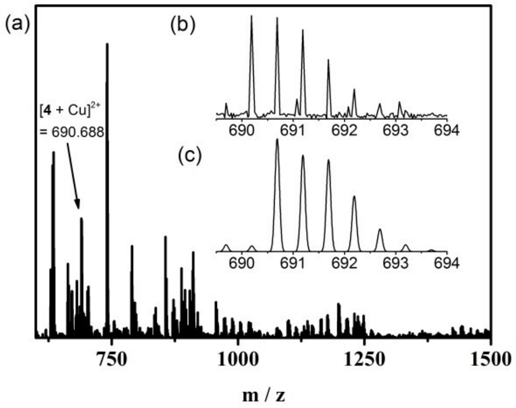

Figure S44. (a) The experimental ESI-MS+ (positive mode) results showing **4** in acetonitrile with the presence of Cu^{2+}. (b) Partial spectrum of the molecular ion of **4**·Cu with an overall of 2+ charge. (c) Theoretical isotopic pattern of the Cu^{2+} complexed to conjugate **4** assigned to [**4** + Cu]$^{2+}$.

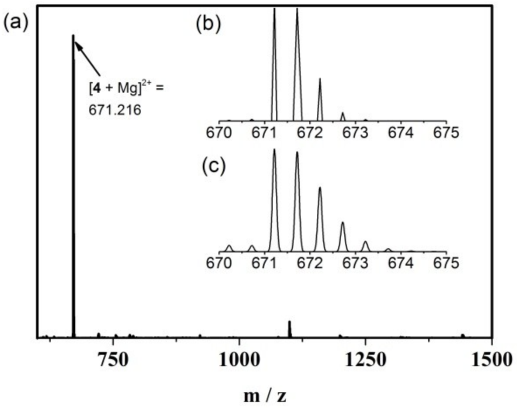

Figure S45. (a) The experimental ESI-MS+ (positive mode) results showing **4** in acetonitrile with the presence of Mg^{2+}. (b) Partial spectrum of the molecular ion of **4**·Mg with an overall of 2+ charge. (c) Theoretical isotopic pattern of the Mg^{2+} complexed to conjugate **4** assigned to [**4** + Mg]$^{2+}$.

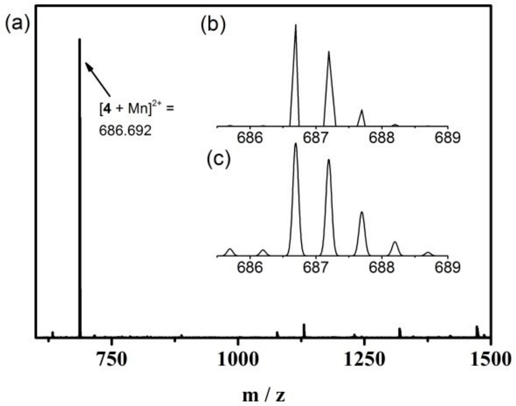

Figure S46. (a) The experimental ESI-MS+ (positive mode) results showing **4** in acetonitrile with the presence of Mn^{2+}. (b) Partial spectrum of the molecular ion of **4**·Mn with an overall of 2+ charge. (c) Theoretical isotopic pattern of the Mn^{2+} complexed to conjugate **4** assigned to [**4** + Mn]$^{2+}$.

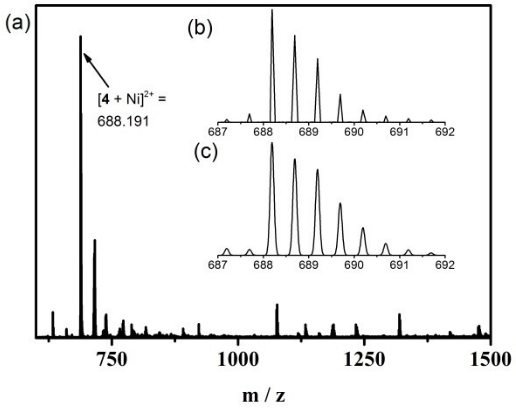

Figure S47. (a) The experimental ESI-MS+ (positive mode) results showing **4** in acetonitrile with the presence of Ni^{2+}. (b) Partial spectrum of the molecular ion of **4**·Ni with an overall of 2+ charge. (c) Theoretical isotopic pattern of the Ni^{2+} complexed to conjugate **4** assigned to [**4** + Ni]$^{2+}$.

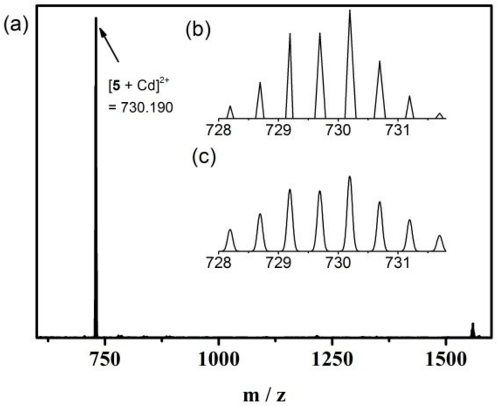

Figure S48. (a) The experimental ESI-MS+ (positive mode) results showing **5** in acetonitrile with the presence of Cd^{2+}. (b) Partial spectrum of the molecular ion of **5**·Cd with an overall of 2+ charge. (c) Theoretical isotopic pattern of the Cd^{2+} complexed to conjugate **5** assigned to [**5** + Cd]$^{2+}$.

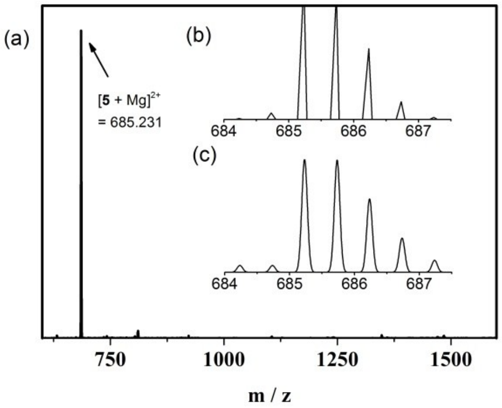

Figure S49. (a) The experimental ESI-MS+ (positive mode) results showing **5** in acetonitrile with the presence of Mg^{2+}. (b) Partial spectrum of the molecular ion of **5**·Mg with an overall of 2+ charge. (c)

Theoretical isotopic pattern of the Mg^{2+} complexed to conjugate **5** assigned to $[\mathbf{5} + Mg]^{2+}$.

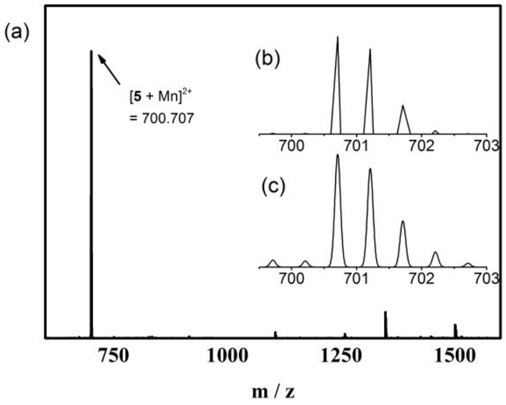

Figure S50. (a) The experimental ESI-MS+ (positive mode) results showing **5** in acetonitrile with the presence of Mn^{2+}. (b) Partial spectrum of the molecular ion of **5**·Mn with an overall of 2+ charge. (c) Theoretical isotopic pattern of the Mn^{2+} complexed to conjugate **5** assigned to $[\mathbf{5} + Mn]^{2+}$.

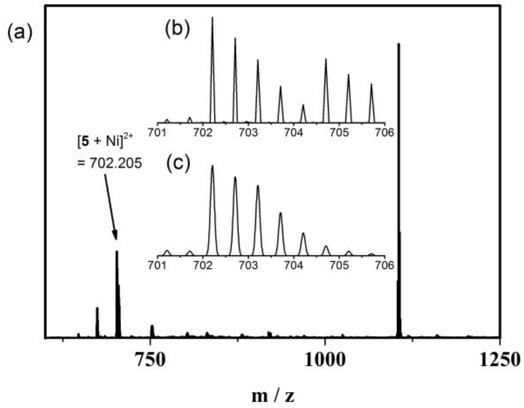

Figure S51. (a) The experimental ESI-MS+ (positive mode) results showing **5** in acetonitrile with the presence of Ni^{2+}. (b) Partial spectrum of the molecular ion of **5**·Ni with an overall of 2+ charge. (c) Theoretical isotopic pattern of the Ni^{2+} complexed to conjugate **5** assigned to $[\mathbf{5} + Ni]^{2+}$.

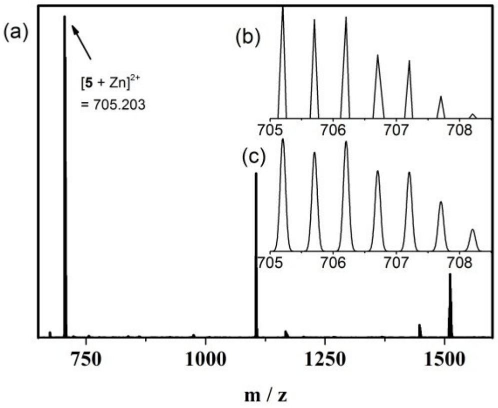

Figure S52. (a) The experimental ESI-MS+ (positive mode) results showing **5** in acetonitrile with the presence of Zn^{2+}. (b) Partial spectrum of the molecular ion of **5**·Zn with an overall of 2+ charge. (c) Theoretical isotopic pattern of the Zn^{2+} complexed to conjugate **5** assigned to [**5** + Zn]$^{2+}$.

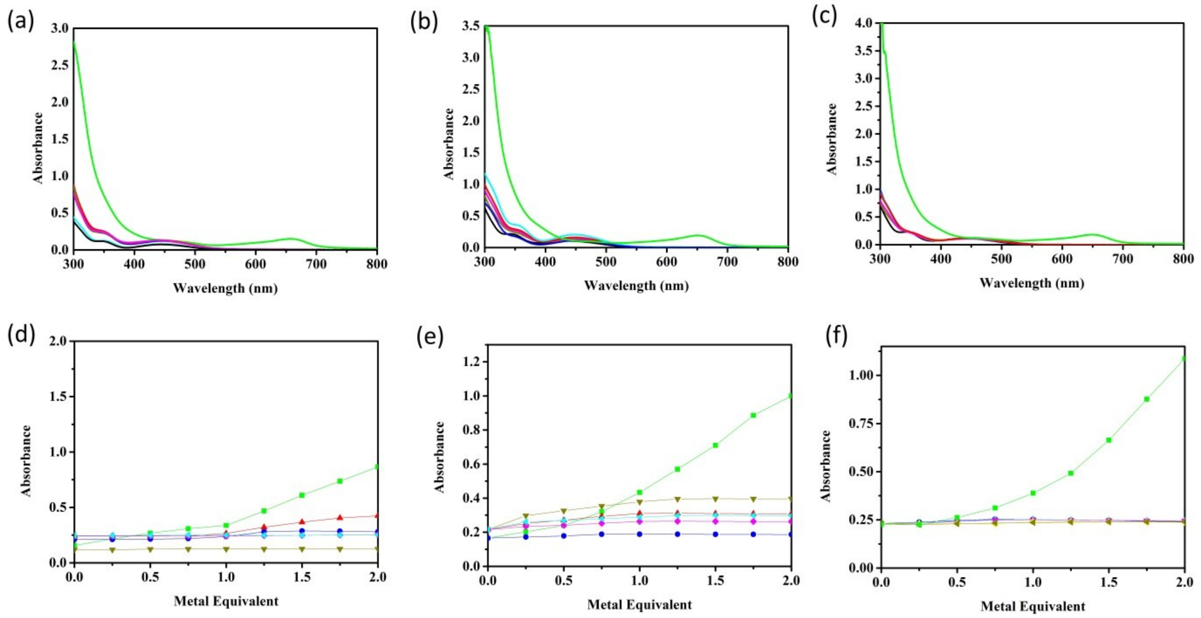

Figure S53. UV spectra of Fc-conjugate **3**, **4**, and **5** shown as a solid black line in (a), (b), and (c), respectively. Changes in the absorbance at wavelength of 342 nm as a function of perchlorate salts: Mg^{2+} (cyan), Mn^{2+} (magenta), Cu^{2+} (green), Zn^{2+} (blue), Ni^{2+} (dark yellow), and Cd^{2+} (red) were monitored. Note that after the addition of 1 equiv. of each metal to each Fc-conjugate **3**(d), **4**(e), and **5**(f), no additional changes in absorbance were observed, except in the presence of Cu^{2+} as no additional changes were detected after 2 equivalence.

Figure S54. Two-dimensional ^{1}H-^{1}H NOEY NMR spectrum of Fc[CO-His(Trt)-His(Trt)-OMe]$_2$ (**3**)

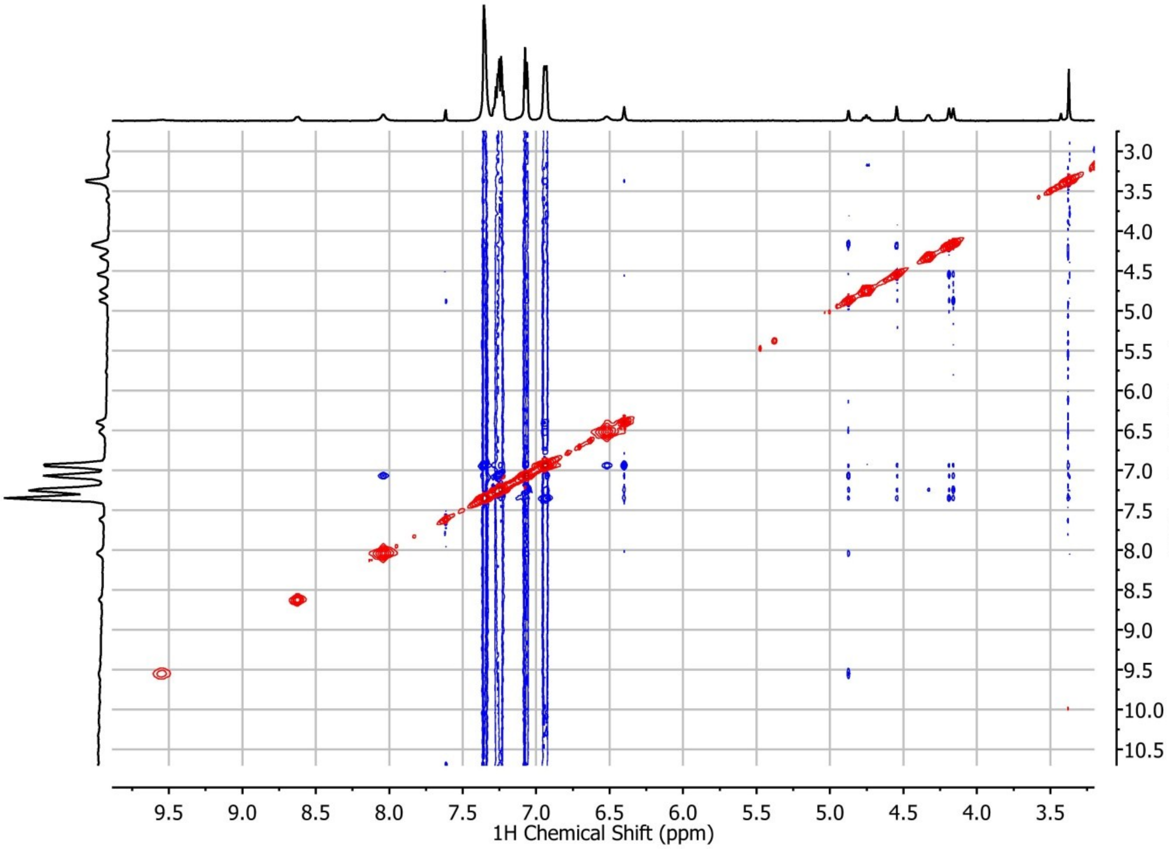

NOESY Experimental Parameters:

The NOESY spectrum was acquired using a 13us 90 degree pulse, 2s recycle delay, 8k data points in the direct dimension and 256 increments under phase sensitive mode. The spectral width for both dimensions was set at 20 ppm. The spectrum was processed using a sine-bell function for both dimensions.

A series of NOESY experiments were performed using different mixing time of 200 ms, 850 ms and 1s. Comparing the spectra at two different mixing times of 1s and 850, we observed that both spectra are nearly identical other the difference in signal to noise. This is due to relaxation of proton. In addition, the sign of the cross peak is opposite of the diagonal, which indicates that the system is in the small molecule regime. This is consistent with the MW of the molecules.

Table S1. Summary of specific angles (°) for the X-ray crystal structures

	Fc-conjugate **4** His-Asp		Fc-conjugate **5** His-Glu	
	Molecule A	Molecule B	Molecule A	Molecule B
θ	2.3(7)	2.8(4)	1.6(2)	3.3(2)
ω	73.3(11)	76.0(11)	76.8(4)	74.8(4)
β	C1A = 3.6(14) at C6A = 5.3(10)	C1B = 6.5(11) at C6B = 2.4(1)	C1A = 3.6(2) at C6A = 6.6(4)	C1B = 5.2(3) at C6B = 5.0(2)

Table S2. Summary of crystallographic data for Fc-conjugates **4** and **5**.

	Fc-conjugate **4**	Fc-conjugate **5**
Empirical formula	$C_{154}H_{149}Fe_2N_{19}O_{24}$	$C_{158}H_{157}Fe_2N_{19}O_{24}$
Formula weight	2761.61	2817.72
Temperature	147(2) K	147(2) K
Wavelength	1.54178 Å	1.54178 Å
Crystal system	Tetragonal	Orthorhombic
Space group	$P4_1$	$P2_12_12_1$
Unit cell dimensions	a = 21.9756(4) Å; α= 90°.	a = 20.9646(5) Å; α= 90°.
	b = 21.9756(4) Å; β= 90°.	b = 22.0475(5) Å; β= 90°.
	c = 30.3333(9) Å; γ = 90°.	c = 31.1954(7) Å;γ = 90°.
Volume	14648.8(7) Å^3	14419.0(6) Å^3
Z	4	4
Density (calculated)	1.252 Mg/m^3	1.298 Mg/m^3
Absorption coefficient	2.199 mm^{-1}	2.244 mm^{-1}
F(000)	5800	5928
Crystal size	0.200 x 0.100 x 0.100 mm^3	0.190 x 0.150 x 0.080 mm^3
Theta range for data collection	2.010 to 67.627°.	2.454 to 67.384°.
Index ranges	-26<=h<=26, -26<=k<=26, -35<=l<=36	-24<=h<=24, -26<=k<=26, -37<=l<=35
Reflections collected	287856	309985
Independent reflections	24883 [R(int) = 0.2357]	25375 [R(int) = 0.0653]
Completeness to theta	= 67.627°; 97.3 %	= 67.384°; 99.4 %
Absorption correction	Semi-empirical from equivalents	Semi-empirical from equivalents
Max. and min. transmission	0.6990 and 0.5434	0.7325 and 0.6209
Refinement method	Full-matrix least-squares on F^2	Full-matrix least-squares on F^2
Data / restraints /	24883 / 1 / 1793	25375 / 3 / 1854

parameters		
Goodness-of-fit on F^2	1.012	1.032
Final R indices [I>2sigma(I)]	R1 = 0.1109, wR2 = 0.2713	R1 = 0.0533, wR2 = 0.1422
R indices (all data)	R1 = 0.1400, wR2 = 0.2975	R1 = 0.0586, wR2 = 0.1458
Absolute structure parameter	0.053(9)	0.021(4)
Extinction coefficient	n/a	n/a
Largest diff. peak and hole	1.819 and -0.720 e.Å^{-3}	0.991 and -0.664 e.Å^{-3}

Table S3. Torsion Angles (deg) for **4** and **5**

Fc-conjugate **4** Molecule A	Atom 1	Atom 2	Atom 3	Atom 4	Torsion Angle (°)
φ_1	C11A	N1A	C12A	C13A	-73(1)
φ_2	C13A	N2A	C14A	C15A	-170.1(9)
φ_3	C43A	N5A	C44A	C45A	-72(1)
φ_4	C45A	N6A	C46A	C47A	-80(1)
ψ_1	N1A	C12A	C13A	N2A	134.1(8)
ψ_2	N5A	C44A	C45A	N6A	140.8(8)
ω_1	C14A	N2A	C13A	C12A	179.4(8)
ω_2	C46A	N6A	C45A	C44A	179.8(8)
Fc-conjugate **4** Molecule B					
φ_1	C11B	N1B	C12B	C13B	-83(1)
φ_2	C13B	N2B	C14B	C15B	-161.0(9)
φ_3	C43B	N5B	C44B	C45B	-74(1)
φ_4	C45B	N6B	C46B	C47B	-89(1)
ψ_1	N1B	C12B	C13B	N2B	135.3(9)
ψ_2	N5B	C44B	C45B	N6B	140.4(9)
ω_1	C14B	N2B	C13B	C12B	-179.2(8)
ω_2	C46B	N6B	C45B	C44B	162(1)
Fc-conjugate **5** Molecule A	Atom 1	Atom 2	Atom 3	Atom 4	Torsion Angle
φ_1	C11A	N1A	C12A	C13A	-73.9(5)
φ_2	C13A	N2A	C14A	C15A	-141.5(4)
φ_3	C44A	N5A	C45A	C46A	-72.8(5)
φ_4	C46A	N6A	C47A	C48A	-123.9(4)
ψ_1	N1A	C12A	C13A	N2A	142.7(4)
ψ_2	N5A	C45A	C46A	N6A	133.8(4)
ω_1	C14A	N2A	C13A	C12A	-176.5(4)
ω_2	C47A	N6A	C46A	C45A	-173.1(4)
Fc-conjugate **5** Molecule B					
φ_1	C11B	N1B	C12B	C13B	-67.5(5)
φ_2	C13B	N2B	C14B	C15B	-143.1(5)
φ_3	C44B	N5B	C45B	C46B	-83.9(5)
φ_4	C46B	N6B	C47B	C48B	-128.7(9)
ψ_1	N1B	C12B	C13B	N2B	133.5(4)
ψ_2	N5B	C45B	C46B	N6B	155.6(4)
ω_1	C14B	N2B	C13B	C12B	-180.0(4)
ω_2	C47B	N6B	C46B	C45B	-178.1(4)

Table S4. CV results of 1 mM compound **3**, **4** and **5** under different scan rates in CH_3CN (0.1 M TBAP as electrolyte)

Fc-peptide	**Scan Rate ($V\cdot s^{-1}$)**	**0.01**	**0.03**	**0.05**	**0.07**	**0.1**	**0.2**	**0.3**	**0.4**	**0.5**	**0.6**
3	$Ep_{1/2}$ / V	0.818	0.828	0.830	0.829	0.834	0.827	0.828	0.827	0.828	0.827
	i_{pa} / i_{pc}	1.46	1.32	1.26	1.22	1.16	1.16	1.17	1.18	1.20	1.21
4	$Ep_{1/2}$ / V	0.851	0.858	0.858	0.860	0.855	0.856	0.857	0.855	0.852	0.85
	ip_a / ip_c	1.67	1.35	1.23	1.24	1.14	1.14	1.14	1.147	1.15	1.16
5	$Ep_{1/2}$ / V	0.848	0.851	0.851	0.860	0.845	0.845	0.846	0.845	0.844	0.846
	ip_a / ip_c	1.39	1.16	1.12	1.13	1.13	1.05	1.07	1.07	1.10	1.12

Table S5. Electrochemical properties of Fc-peptides **3-5**. Summary of electrochemical results: half-wave potentials [$E_{1/2}$, mV], peak separation [ΔE_p, mV], diffusion coefficients of oxidized and reduced species [D_O and D_R, cm^2/s] and heterogeneous electron transfer rate constant [k_{sh}, cm/s] of Fc-peptides **3-5** obtained by corresponding CV/SWV measurements. Concentration of Fc-peptides were 1.0 mM with 0.1 M TBAP as a supporting electrolyte. Glassy carbon working electrode, Pt wire counter electrode, and Ag/AgCl as reference electrode were used.

Fc-peptide	$E_{1/2}$	ΔE_p	$E_{1/2}$	D_O	D_R	k_{sh}
	CV	CV	SWV	($x10^{-7}$)	($x10^{-7}$)	($x10^{-2}$)
3	834	76	836	1.53	0.663	2.73
4	855	75	853	1.36	0.207	2.58
5	845	68	848	1.10	0.478	3.47

Table S6. Summary of electrochemical data: half-wave potentials [$E_{1/2}$, mV], change in half-wave potentials [$\Delta E_{1/2}$, mV] and peak separation [ΔE, mV] of Fc-conjugates **3-5** obtained from CV. TBAP (0.1mM) was added as supporting electrolyte. Glassy carbon working electrode, Pt wire counter electrode, and Ag/AgCl reference electrode were used.

Fc-peptide	**3**				**4**				**5**			
	$E_{1/2}$/ mV	$\Delta E_{1/2}$/ mV	ΔEp/ mV	ΔG / kJ· mol^{-1}	$E_{1/2}$/ mV	$\Delta E_{1/2}$/ mV	ΔEp/ mV	ΔG / kJ· mol^{-1}	$E_{1/2}$/ mV	$\Delta E_{1/2}$/ mV	ΔEp/ mV	ΔG / kJ· mol^{-1}
No Metal	834	-	76	-7.3	855	-	75	-7.2	846	-	68	-6.6
Cu^{2+}	949	115	189	-18.2	914	59	109	-10.5	889	44	138	-13.3
Zn^{2+}	923	89	145	-14.0	910	55	162	-15.6	885	39	91	-8.8
Ni^{2+}	910	76	207	-20.0	907	51	144	-13.9	871	25	124	-12.0
Cd^{2+}	908	74	197	-19.0	899	44	145	-14.0	870	24	111	-10.7
Mn^{2+}	902	69	214	-20.6	897	42	125	-12.1	864	18	131	-12.6
Mg^{2+}	901	67	155	-15.0	883	28	129	-12.4	859	13	86	-8.3

Table S7: Results of the high resolution electrospray mass spectrometry analysis of acetonitrile solutions containing Fc-conjugates **3** and **5** the absence and presence of metal ions.

Complex Composition	Mass	Calculated Mass
3	[M + H]$^+$ = 1820.6921	[M + H]$^+$ = 1820.7099
3 and Zn^{2+}	[M + Zn]$^{2+}$ = 942.3125	[M + Zn]$^{2+}$ = 942.3153
3 and Cd^{2+}	[M + Cd]$^{2+}$ = 966.3011	[M + Cd]$^{2+}$ = 966.3040
3 and Ni^{2+}	[M + Ni]$^{2+}$ = 938.8171	[M + Ni]$^{2+}$ = 938.8184
3 and Cu^{2+}	-	[M + Cu]$^{2+}$ = 944.3384
3 and Mg^{2+}	[M + Mg]$^{2+}$ = 922.8423	[M + Mg]$^{2+}$ = 922.8511
3 and Mn^{2+}	[M + Mn]$^{2+}$ = 937.3200	[M + Mn]$^{2+}$ = 937.8237
5	[M + H]$^+$ = 1347.4842	[M + H]$^+$ = 1347.4845
5 and Zn^{2+}	[M + Zn]$^{2+}$ = 705.2030	[M + Zn]$^{2+}$ = 705.2051
5 and Cd^{2+}	[M + Cd]$^{2+}$ = 730.1896	[M + Cd]$^{2+}$ = 730.1887
5 and Ni^{2+}	[M + Ni]$^{2+}$ = 702.2048	[M + Ni]$^{2+}$ = 702.2082
5 and Cu^{2+}	-	[M + Cu]$^{2+}$ = 704.7054
5 and Mg^{2+}	[M + Mg]$^{2+}$ = 685.2314	[M + Mg]$^{2+}$ = 685.2331
5 and Mn^{2+}	[M + Mn]$^{2+}$ = 700.7072	[M + Mn]$^{2+}$ = 700.7096

Table S8. Summary of IR stretching frequencies (cm^{-1})

IR stretching frequencies of C=O amide (cm^{-1})					
Compound	NH	NH’	C=O ester	C=O’ amide	C=O amide
3	3315	3057	1738	1640	1537
3 and Cu^{2+}	3322	3059	1741	1641	1526
3 and Zn^{2+}	3305	3059	1740	1646	1532
3 and Cd^{2+}	3347	3060	1743	1639	1529
3 and Ni^{2+}	3322	3059	1741	1637	1524
3 and Mg^{2+}	3322	3059	1740	1632	1533
3 and Mn^{2+}	3306	3059	1741	1649	1534
4	3306	3057	1739	1650	1542
4 and Cu^{2+}	3514	3057	1742	1625	1525
4 and Zn^{2+}	3513	3102	1738	1629	1525
4 and Cd^{2+}	3496	3057	1729	1618	1530
4 and Ni^{2+}	3481	3117	1743	1636	1515
4 and Mg^{2+}	3514	3057	1731	1636	1532
4 and Mn^{2+}	3513	3093	1738	1630	1524
5	3323	3088	1735	1649	1543
5 and Cu^{2+}	3527	3263	1739	1626	1510
5 and Zn^{2+}	3503	3251	1740	1625	1525
5 and Cd^{2+}	3457	3164	1741	1633	1519
5 and Ni^{2+}	3488	3260	1739	1626	1517
5 and Mg^{2+}	3548	3088	1728	1632	1527
5 and Mn^{2+}	3545	3088	1736	1633	1523

Table S9: UV and CD spectroscopic parameters for Fc–peptide conjugate **3** and **5**

Compound	UV-Vis (nm(ε))	λ/nm (M_{Θ}/deg $mM^{-1}\cdot cm^{-1}$)
3	341(0.20)	470(-3.6)
3·Cu^{2+}	343(0.23)	495(-1.1)
3·Zn^{2+}	341(0.29)	492(-2.5)
3·Cd^{2+}	342(0.43)	470(-2.2)
3·Ni^{2+}	341(0.25)	482(-2.4)
3·Mg^{2+}	347(0.23)	482(-2.2)
3·Mn^{2+}	344(0.25)	480(-2.2)
5	341(0.19)	487(+4.1)
5·Cu^{2+}	342(0.47)	513(+1.2)
5·Zn^{2+}	345(0.26)	568(+1.4)
5·Cd^{2+}	343(0.25)	568(+0.4)
5·Ni^{2+}	344(0.24)	508(+1.4)
5·Mg^{2+}	342(0.25)	572(+0.7)
5·Mn^{2+}	342(0.25)	509(+0.3)